Title
The soil water characteristic as new class of closed-form parametric expressions for the flow duration curve

Authors
Sadegh, M
Vrugt, JA
Gupta, HV
et al.

Publication Date
2016-04-01

DOI
10.1016/j.jhydrol.2016.01.027

Peer reviewed

Journal of Hydrology 535 (2016) 438–456

Contents lists available at ScienceDirect

Journal of Hydrology

journal homepage: www.elsevier.com/locate/jhydrol

The soil water characteristic as new class of closed-form parametric expressions for the flow duration curve

M. Sadegh [a], J.A. Vrugt [a,b,*], H.V. Gupta [c], C. Xu [d]

[a] Department of Civil and Environmental Engineering, University of California, Irvine, USA
[b] Department of Earth System Science, University of California, Irvine, CA, USA
[c] Department of Hydrology and Water Resources, University of Arizona, Tucson, CA, USA
[d] Los Alamos National Laboratory, Los Alamos, NM, USA

ARTICLE INFO

Article history:
Received 25 August 2015
Received in revised form 6 January 2016
Accepted 14 January 2016
Available online 23 January 2016
This manuscript was handled by Peter K. Kitanidis, Editor-in-Chief, with the assistance of Christophe Darnault, Associate Editor

Keywords:
Closed-form expression for FDC
Soil water characteristic
Regionalization of FDC

SUMMARY

The flow duration curve is a signature catchment characteristic that depicts graphically the relationship between the exceedance probability of streamflow and its magnitude. This curve is relatively easy to create and interpret, and is used widely for hydrologic analysis, water quality management, and the design of hydroelectric power plants (among others). Several mathematical expressions have been proposed to mimic the FDC. Yet, these efforts have not been particularly successful, in large part because available functions are not flexible enough to portray accurately the functional shape of the FDC for a large range of catchments and contrasting hydrologic behaviors. Here, we extend the work of Vrugt and Sadegh (2013) and introduce several commonly used models of the soil water characteristic as new class of closed-form parametric expressions for the flow duration curve. These soil water retention functions are relatively simple to use, contain between two to three parameters, and mimic closely the empirical FDCs of 430 catchments of the MOPEX data set. We then relate the calibrated parameter values of these models to physical and climatological characteristics of the watershed using multivariate linear regression analysis, and evaluate the regionalization potential of our proposed models against those of the literature. If quality of fit is of main importance then the 3-parameter van Genuchten model is preferred, whereas the 2-parameter lognormal, 3-parameter GEV and generalized Pareto models show greater promise for regionalization.

1. Introduction

The flow duration curve (FDC) is a widely used characteristic signature of a watershed, and is one of the three most commonly used graphical methods in hydrologic studies, along with the mass curve and the hydrograph (Foster, 1934). The FDC relates the exceedance probability (frequency) of streamflow to its magnitude, and characterizes both the flow regime and the streamflow variability of a watershed. It is closely related to the "survival" function in statistics (Vogel and Fennessey, 1994), and is interpreted as a complement to the streamflow cumulative distribution function (CDF). The FDC is frequently used to predict the distribution of streamflow for water resources planning purposes, to simplify analysis of water resources problems, and to communicate watershed behavior to those who lack in-depth hydrologic knowledge. One should be particularly careful to rely solely on the FDC as main descriptor of catchment behavior (Vogel and Fennessey, 1995; Westerberg et al., 2014) as the curve represents the rainfall-runoff as disaggregated in the time domain and hence lacks temporal structure (Searcy, 1959; Vogel and Fennessey, 1994).

The first application of the FDC dates back to 1880 and appears in the work by Clemens Herschel (Foster, 1934). Ever since, the FDC has been used in many fields of study including (among others) the design and operation of hydropower plants (Singh et al., 2001; Niadas and Mentzelopoulos, 2008), flow diversion and irrigation planning (Chow, 1964; Warnick, 1984; Pitman, 1993; Mallory and McKenzie, 1993), streamflow assessment and prediction (Tharme, 2003), sedimentation (Vogel and Fennessey, 1995), water quality management (Mitchell, 1957; Searcy, 1959; Jehng-Jung and Bau, 1996; Moftakhari et al., 2015), waste-water treatment design (Male and Ogawa, 1984), and low-flow analysis (Wilby et al., 1994; Smakhtin, 2001; Pfannerstill et al., 2014). Recent studies have used the FDC as a benchmark for quality control (Cole et al., 2003),

* Corresponding author at: Department of Civil and Environmental Engineering, University of California, Irvine, USA.
E-mail addresses: msadegh@uci.edu (M. Sadegh), jasper@uci.edu (J.A. Vrugt), hoshin.gupta@hwr.arizona.edu (H.V. Gupta), xcu@lanl.gov (C. Xu).

http://dx.doi.org/10.1016/j.jhydrol.2016.01.027
0022-1694/

and signature or metric for model calibration and evaluation (Refsgaard and Knudsen, 1996; Yu and Yang, 2000; Wagener and Wheater, 2006; Son and Sivapalan, 2007; Yadav et al., 2007; Yilmaz et al., 2008; Zhang et al., 2008; Blazkova and Beven, 2009; Westerberg et al., 2011; Vrugt and Sadegh, 2013; Pfannerstill et al., 2014; Sadegh and Vrugt, 2014; Sadegh et al., 2015). For instance, Vrugt and Sadegh (2013) used the fitting coefficients of a simple parametric expression of the FDC as summary statistics in diagnostic model calibration and evaluation using approximate Bayesian computation (ABC). This ABC diagnostics methodology has been introduced and described by Vrugt and Sadegh (2013) and interested readers are referred to this and subsequent publications by Sadegh and Vrugt (2014), Sadegh et al. (2015), Vrugt (2016) for further details.

Application of FDCs for hypothesis testing (Kavetski et al., 2011) can improve identifiability and help attenuate the problems associated with traditional residual-based objective (likelihood) functions (e.g. Nash–Sutcliffe, sum of squared residuals, absolute error, relative error) that emphasize fitting specific parts of the hydrograph, such as high or low flows (Schaefli and Gupta, 2007; Kavetski et al., 2011; Westerberg et al., 2011), and thereby lose important information regarding the structural inadequacies of the model (Gupta et al., 2008, 2012; Vrugt and Sadegh, 2013). The FDC is a signature watershed characteristic that along with other hydrologic metrics, can help shed lights on epistemic (model structural) errors (Euser et al., 2013; Vrugt and Sadegh, 2013). For example, Son and Sivapalan (2007) used the FDC to highlight the reasons of model malfunctioning and to propose improvements to the structure of their conceptual water balance model for the watershed under investigation. Indeed, a deep groundwater flux was required to simulate adequately dominant low flows of the hydrograph. Yilmaz et al. (2008) in a similar effort to improve simulation of the vertical distribution of soil moisture in the HL-DHM model, used the slope of the FDC as benchmark for model performance. The FDC was deemed suitable for this purpose due to its strong dependence on the simulated soil moisture distribution, and relative lack of sensitivity to rainfall data and timing errors. However, the proposed refinements of the HL-DHM model were found inadequate and this failure was attributed to the inherent weaknesses of the conceptual structure of HL-DHM.

The usefulness of duration curves (e.g. precipitation (Yokoo and Sivapalan, 2011), baseflow (Kunkle, 1962) and streamflow (flow) (Hughes and Smakhtin, 1996)) depends in large part on the temporal resolution of the data (e.g. quarterly, hourly, daily, weekly, and monthly) these curves are constructed from. FDCs derived from daily streamflow data are commonly considered to warrant an adequate analysis of the hydrologic response of a watershed (Vogel and Fennessey, 1994; Smakhtin, 2001; Wagener and Wheater, 2006; Zhao et al., 2012). For example, a FDC with a steep mid section (also referred to as slope) is characteristic for a watershed that responds quickly to rainfall, and thus has a small storage capacity and large ratio of direct runoff to baseflow. A more moderate slope, on the contrary, is indicative of a basin whose streamflow response reacts much slower to precipitation forcing with discharge that is made up in large part of baseflow (Yilmaz et al., 2008).

The shape of the FDC is determined by several factors including (amongst others) topography, physiography, climate, vegetation cover, land use, and storage capacity (Singh, 1971; Lane et al., 2005; Zhao et al., 2012; Brown et al., 2013), and can be used to perform regional analysis (Wagener and Wheater, 2006; Masih et al., 2010) or to cluster catchments into relatively homogeneous groups that exhibit a relatively similar hydrologic behavior (Sawicz et al., 2011; Coopersmith et al., 2012). Different studies have appeared in the hydrologic literature that have analyzed how the shape of the FDC is affected by physiographic factors and/or vegetation cover. Despite this progress made, interpretation of the FDC can be controversial if an insufficiently long streamflow data record is used (Vogel and Fennessey, 1994). The lower end of the FDC (low flows) is particularly sensitive to the period of study, and to whether the streamflow data includes severe droughts or not (Castellarin et al., 2004a). If the available data is sparse and does not warrant an accurate description of the FDC, then the use of an annual duration curve is advocated (Searcy, 1959; Vogel and Fennessey, 1994; Castellarin et al., 2004a,b). This curve describes the relationship between the magnitude and frequency of the streamflow for a "typical hypothetical year" (Vogel and Fennessey, 1994). To construct an annual FDC, the available data is divided into z years and individual FDCs are constructed for each year. Then, for each exceedance probability a median streamflow is derived from these z different FDCs and used to create the annual FDC. Vogel and Fennessey (1994) used this concept to associate confidence and recurrence intervals to FDCs in a nonparametric framework. One should note that the FDC of the total data record is, in general, more accurate than the annual FDC (Leboutillier and Waylen, 1993). What is more, recent studies have provided physically-based approaches, especially for tidal rivers, to extend river discharge records beyond the period of observation (Moftakhari et al., 2013; Moftakhari, 2015). Such approaches can be helpful to derive the FDC for sites with scarce or no discharge observations.

To better analyze and understand the physical controls on the FDC, it is common practice to divide the total FDC (TFDC) into a slow (SFDC) and fast (FFDC) flow component (Yokoo and Sivapalan, 2011; Cheng et al., 2012; Coopersmith et al., 2012; Yaeger et al., 2012; Ye et al., 2012). For example, Yokoo and Sivapalan (2011) concluded from numerical simulations with a simple water balance model that the FFDC is controlled mainly by precipitation events and timing, whereas the SFDC is most sensitive to the storage capacity of the watershed and its baseflow response. This type of analysis is of particular value in regionalization studies, and prediction in ungauged basins. Indeed, much effort has gone towards prediction of the FDC in ungauged basins using measurements of the rainfall-runoff response from hydrologically similar, and preferably geographically nearby, gauged basins (Holmes et al., 2002; Sivapalan et al., 2003).

In this context, one approach has been to cluster catchments into classes with similar physiographic and climatic characteristics, and then to estimate dimensionless (non-parametric) FDCs for gauged basins which in turn are then applied to ungauged basins (Niadas, 2005; Ganora et al., 2009). One such example is the work of Pugliese et al. (2014) who applied top-kriging to predict the empirical FDC in ungauged catchments. The FDCs are normalized by an index value (e.g. mean annual runoff) to generate dimensionless curves (Ganora et al., 2009; Shamseldin, 2014). A detailed review on methods for clustering of homogeneous catchments appears in Sauquet and Catalogne (2011) and Booker and Snelder (2012), and interested readers are referred to these publications for more information. Another approach has been to mimic the empirical (observed) FDC with a mathematical/probabilistic model and to correlate the fitting coefficients of such parametric expressions to physical and climatological characteristics of the watershed using regression techniques, index models, artificial intelligence, and spacial interpolation schemes (Fennessey and Vogel, 1990; Yu and Yang, 1996; Yu et al., 2002; Croker et al., 2003; Castellarin et al., 2004a,b, 2007; Li et al., 2010; Sauquet and Catalogne, 2011; Viola et al., 2011; Longobardi and Villani, 2013; Pumo et al., 2013; Mendicino and Senatore, 2013; Shamseldin, 2014; Waseem et al., 2015). Such pedotransfer functions can then be used to predict the FDC of ungauged basins from simple catchment data (e.g. soil texture, topography, vegetation cover, etc.).

Models that emulate the FDC can be grouped in two main classes: 1. Physical models that use physiographic and climatic characteristics of the watersheds (e.g. drainage area, mean areal

precipitation, soil properties, etc.) as parameters of the FDC (Singh, 1971; Dingman, 1978; Yu and Yang, 1996; Holmes et al., 2002; Yu et al., 2002; Lane et al., 2005; Botter et al., 2008; Mohamoud, 2008) and 2. Probabilistic/mathematical functions that use between two to five fitting coefficients to mimic the empirical FDC as closely and consistently as possible (Quimpo et al., 1983; Mimikou and Kaemaki, 1985; Fennessey and Vogel, 1990; Leboutillier and Waylen, 1993; Franchini and Suppo, 1996; Cigizoglu and Bayazit, 2000; Croker et al., 2003; Botter et al., 2008; Li et al., 2010; Booker and Snelder, 2012).

The early work of Dingman (1978) is the first study that used physical models to mimic empirical FDCs. Topography maps were used as signature of catchment behavior to predict the FDC using relatively simple first-order polynomial functions. Two more recent studies by Yu and Yang (1996), and Yu et al. (2002) used similar regression functions to predict the FDC of catchments in Taiwan but considered the drainage area as main proxy of the rainfall-runoff transformation.

Probabilistic methods include the use of lognormal and lognormal mixture (Fennessey and Vogel, 1990; Leboutillier and Waylen, 1993; Castellarin et al., 2004a; Li et al., 2010), generalized Pareto (Castellarin et al., 2004b), generalized extreme value, gamma and Gumbel (Booker and Snelder, 2012), beta (Iacobellis, 2008), and logistic distributions (Castellarin et al., 2004b). Other mathematical models include (amongst others) the use of exponential, power, logarithmic (Quimpo et al., 1983; Franchini and Suppo, 1996; Lane et al., 2005; Booker and Snelder, 2012), and polynomial functions (Mimikou and Kaemaki, 1985; Yu et al., 2002). Detailed reviews of different functions for the FDC can be found in Sauquet and Catalogne (2011), Booker and Snelder (2012) and Mendicino and Senatore (2013). In another line of work, Cigizoglu and Bayazit (2000) used convolution theory to predict the FDC as a product of periodic and stochastic streamflow components. What is more, Croker et al. (2003) used probability theory to combine a model that predicts the FDC of days with non-zero streamflow with a distribution function that determines randomly the probability of dry days.

Notwithstanding this progress made, the probabilistic and mathematical functions used in the hydrologic literature fail, usually, to properly mimic all parts of the FDC when benchmarked against watersheds with completely different hydrologic behaviors. Consequently, some researchers focus only on a specific portion of the FDC, commonly the low flows (Fennessey and Vogel, 1990; Franchini and Suppo, 1996), whereas others prefer to use several percentiles of the FDC rather than the entire curve (Lane et al., 2005; Mohamoud, 2008; Blazkova and Beven, 2009). While complex "S" shaped FDCs can only be modeled adequately if a sufficient number of parameters (say five to seven) are used (Ganora et al., 2009), one should be particularly careful using such relatively complex FDC models for regionalization and prediction in ungauged basins as parameter correlation and insensitivity can complicate and corrupt the inference and results.

In this paper, we introduce a new class of closed-form mathematical expressions which are capable of describing the FDCs of a very large number of watersheds with contrasting hydrologic behaviors. We extend the ideas presented in Vrugt and Sadegh (2013), and propose several commonly used functions of the soil water characteristic as mathematical models for the observed (empirical) FDCs. These models have between two to three parameters and describe closely the FDCs of the MOPEX data set. This work is a follow up of Vrugt and Sadegh (2013) who introduced a 2-parameter formulation of the van Genuchten (VG) retention function (van Genuchten, 1980) as model for the FDC. The fitting coefficients of this function were derived by calibration against the observed FDC of the French Broad river basin and used as summary statistics in diagnostic model evaluation with ABC. Here, we extend this preliminary work, and introduce and benchmark several other soil water retention functions (SWRFs) using historical streamflow observations from 430 watersheds of the MOPEX data set. We are particularly interested in the quality of fit of each model, parameter sensitivity and correlation, and regionalization potential of the fitting coefficients.

The motivating idea of this paper is the strong analogy in hydrologic functioning and behavior between a watershed and a porous medium such as a soil. Both are subject to hydroclimatologic forcing (e.g. rainfall, evaporation, transpiration), have an intrinsic ability to retain water (this capacity is due to capillary action, osmotic binding and the presence of London-van der Waals forces acting between the solid phase and water), and transport water in response to gradients in the total (hydraulic) potential (includes effects of gravity and local water availability). This transport of water can take place via different trajectories including fast (e.g. macropores – also called preferential flow), and slow (matrix) flow pathways, and involve the entire range of flow conditions ranging from simple linear/nonlinear laminar flow to turbulent (within stream) transport. This analogy attempt is tailored specifically to surface hydrology to help rectify the chronic historical deficit of physics-based approaches (derived from first-order physical principles) in analyzing the watershed response to rainfall. Related ideas published by Vrugt et al. (2005) have shown how concepts of micromixing borrowed from the field of chemical reaction engineering can be used to model tracer experiments at C-wells near Yucca Mountain, Nevada.

One does not need to agree with our analogy hypothesis to appreciate the findings of this paper. Our hypothesis does open up an arsenal of new mathematical and physically-based approaches to describe large-scale hydrologic behavior. For instance, dual porosity (permeability) approaches allow one to describe preferential flow whereas the mobile/immobile water concept developed (among others) to simulate correctly the tailing behavior of solutes provides a mechanism to describe correctly the residence time distribution of water in the catchment in pursuit of a correct representation of the age distribution of the hydrograph. These ideas provide a powerful alternative to conceptual modeling approaches but have to be supported with much further research and analysis, the outcome of which will be reported in due course. For now, we focus our attention to the use of soil hydraulic models to describe accurately the flow duration curve of a large cohort of watersheds with contrasting hydrologic behaviors. These mathematical expressions can be used (amongst others) for hydrologic modeling, prediction in ungauged basins and regionalization.

The remainder of this paper is organized as follows. Section 2 provides a brief review of the most commonly used probabilistic and empirical models in the literature to mimic the FDC, and introduces several closed-form expressions of the soil water characteristic to emulate FDCs. This section also discusses the MOPEX data set, and the optimization procedure to estimate the values of the fitting coefficients of each SWRF. Then in Section 3, we present and discuss the fitting results of each of the proposed parametric expressions. Here, we are especially concerned with benchmarking of our results against those of the FDC models used in the literature, analysis of parameter sensitivity and correlation. Section 4 evaluates the regionalization potential of each parametric expression of the FDC using multivariate regression analysis of the FDC parameters and basin characteristics. Finally, Section 5 concludes this paper with a summary of the most important findings.

2. Materials and methods

2.1. Experimental data: MOPEX data set

We use daily streamflow data from 438 MOPEX watersheds to analyze the ability of different mathematical functions to fit the

empirical FDCs. This data set has been described by Duan et al. (2006) and is available for public download from the following website: http://ftp://hydrology.nws.noaa.gov/pub/gcip/mopex/US_Data/. This includes watersheds from across the United States with different hydrologic behaviors. The empirical FDCs are constructed using all of the available streamflow data for each watershed. Fig. 1 shows the observed FDCs for eight of the MOPEX watersheds. The discharge values of each watershed (y-axis) are normalized between zero and one so that the FDCs of the watersheds can be compared more easily visually. A large variety in the FDCs of the MOPEX data set is observed. This confirms the need for a flexible function that can adequately describe the large range of hydrologic behaviors.

This rich archive of 438 catchments in the USA contains relatively long records of daily hydrologic data (rainfall, potential evapotranspiration and streamflow). Eight watersheds were excluded from our analysis due to an insufficient number of streamflow observations. The remaining 430 catchments have between 3,773 and 19,997 daily streamflow observations and were used for FDC model testing and evaluation. Fig. 2 provides further insights into the amount of data available for different watersheds, and presents a frequency distribution (histogram) of the length of the data set (days).

2.2. Empirical flow duration curve

The FDC describes the relationship between the magnitude of the streamflow and its exceedance probability. The shape of a flow-duration curve in its upper and lower regions is particularly significant in evaluating the stream and basin characteristics. The shape of the curve in the high-flow region indicates the type of flood regime the basin is likely to have, whereas, the shape of the low-flow region characterizes the ability of the basin to sustain low flows during dry seasons. A very steep curve (high flows for short periods) would be expected for rain-caused floods on small watersheds.

If we denote with $\widehat{\mathbf{Y}} = \{\hat{y}_1, \ldots, \hat{y}_n\}$ the observed record of n discharge values, then we can calculate the exceedance probability of each value of $\widehat{\mathbf{Y}}$ as follows. We first sort the n-vector of $\widehat{\mathbf{Y}}$ in descending order and store vector of discharge values in the vector $\widehat{\mathbf{Y}}_{\text{rms}}$. Each element of this sorted vector is then assigned a rank, $\mathbf{R} = \{1, \ldots, n\}$ starting with one for the largest discharge value (first element of $\widehat{\mathbf{Y}}_{\text{rms}}$). We can now calculate the exceedance probability, e_i of each discharge observation, $i = \{1, \ldots, n\}$ of $\widehat{\mathbf{Y}}_{\text{rms}}$ using the Weibull plotting position

$$\hat{e}_i = \frac{1}{n}\left(r_i - \frac{1}{2}\right), \tag{1}$$

where i denotes the element number of $\widehat{\mathbf{Y}}_{\text{rms}}$ (equivalent to rank), and $\hat{\mathbf{E}} = \{\hat{e}_1, \ldots, \hat{e}_n\}$ signifies the n-vector of corresponding exceedance probabilities. Other formulations of Eq. (1) have been proposed in the statistical literature but provide very similar estimates of the exceedance probabilities for large data records, say $n > 100$.

The FDC is an important signature of the catchment response to rainfall and is relatively easy to construct from the observed discharge record. It only requires a function to sort the discharge data record. One issue, however deserves special attention, and that is the presence of (near)-zero flows. This is common for (dry-bed) ephemeral or intermittent streams in semi-arid watersheds that alternate between short flash-flood events characterized by pronounced runoff dynamics and rapidly rising hydrographs, and long periods of (nearly) zero flows. With treatment of zero flow days the FDC would consist of two different parts, a regular "S"-shaped section between values of the exceedance probability, $\hat{e}_i \in [0, 1 - \hat{p}_0]$ and $\hat{y} > 0$, and a horizontal portion for $\hat{e}_i \in [1 - \hat{p}_0, 1]$ and $\hat{y} = 0$, where $\hat{p}_0$ denotes the probability of zero flows. The value of $\hat{p}_0$ is easily computed from the observed record of discharge values

$$\hat{p}_0 = \frac{n_0}{n} \tag{2}$$

where n_0 signifies the number of zero flow observations. The value of $\hat{p}_0$ is not as much determined by watershed properties (geology, soils, slope, etc.) but rather by climatic conditions (precipitation). In the remainder of this paper, we therefore assume $\hat{p}_0$ to be known for each watershed and use the following variable instead

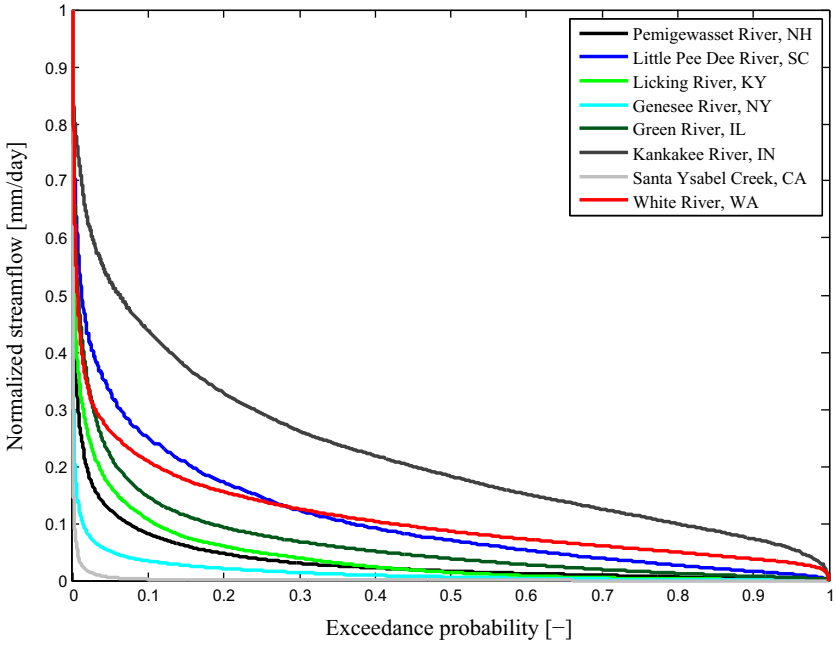

Fig. 1. Flow duration curves of eight watersheds of the MOPEX data set. The streamflow values have been normalized so that they share a common scale and the different empirical FDCs can be compared.

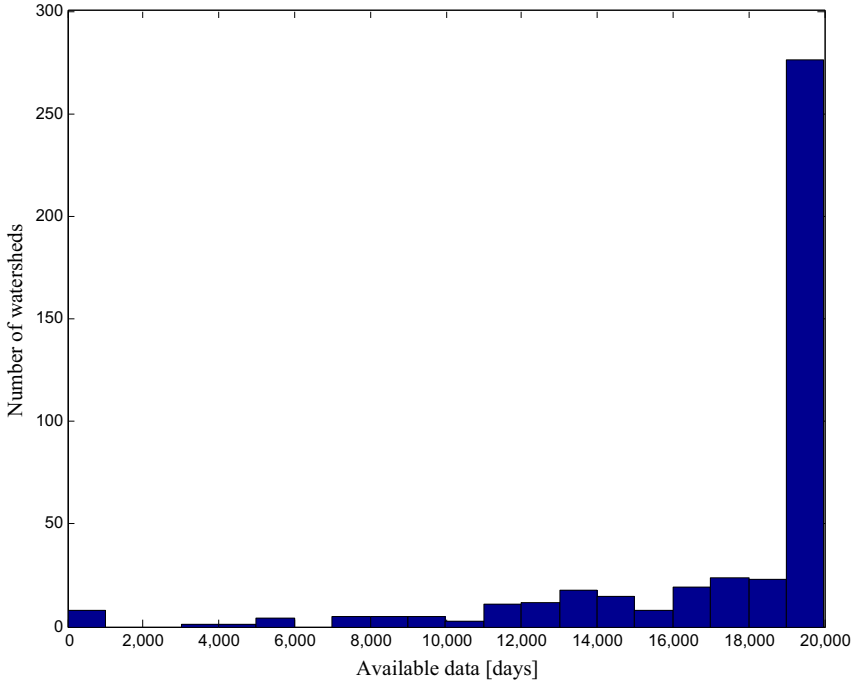

Fig. 2. Histogram of the data length (days) of the MOPEX suite of watersheds.

$$\hat{e}_i^* = \frac{\hat{e}_i}{1-\hat{p}_0}, \tag{3}$$

in our parametric expressions of the FDC. This transformed variable scales linearly the exceedance probabilities of the non-zero flows to the interval $[0,1]$. The exceedance probabilities of the original discharge record are then easily derived by inverting Eq. (3). Note, the majority of the MOPEX data records (>82%) has strictly positive flows, and thus for those watersheds $\hat{p}_0 = 0$ and consequently $\hat{e}_i^* = \hat{e}_i$. In the remainder of this paper, we use the wording "empirical FDC" to denote the n measured $\{\hat{e}_i, \hat{y}_i\}$ pairs of the watershed.

2.3. Probabilistic and mathematical functions

We now review a suite of different functions commonly used in the hydrologic literature to mimic the empirical FDC. These functions can be grouped in two main classes. The first class builds on commonly used probability distributions, and are also referred to in the literature as probabilistic models. The second class of models uses standard parametric expressions to capture the "S"-shaped curve of the FDC. Unlike the first class of models which uses the mathematical equation of the (inverse) CDF, this second group of nonprobabilistic models involves a higher-degree of trial-and-error in their development.

2.3.1. Probabilistic models

This class of models is used widely by researchers and practitioners in large part due to their relative parametric simplicity, flexibility, solid statistical underpinning and relative ease of derivation. Indeed, the probability of exceedence, e, is easily computed from the cumulative distribution function (CDF) as follows

$$e = 1 - p(y \le Y) = 1 - \mathrm{CDF}(y), \tag{4}$$

so that the highest flows (CDF close to unity) are associated with an exceedance probability of zero. Thus, any statistical distribution with a closed-form mathematical expression for its CDF can be easily converted into a model for the FDC. In the remainder of this section, we conveniently refer to the transformation of Eq. (4) as the pseudo-CDF or the pseudo-inverse CDF if variables e and y are switched around.

The first of these models involves the Gumbel distribution (Booker and Snelder, 2012). The skew of the discharge data, so clearly visible in a frequency distribution of the streamflows, prompts the use of this model. The pseudo-inverse CDF of the Gumbel distribution is given by

$$y_i = a_G - b_G \log\left[-\log\left(1-e_i^*\right)\right], \tag{5}$$

where e_i^* denotes the scaled exceedance probability, and a_G (mm/day) and b_G (mm/day) are coefficients that define the location and scale of the Gumbel distribution. Eq. (5) is a special case of the generalized extreme value (GEV) distribution.

$$y_i = a_{GEV} + \frac{b_{GEV}}{c_{GEV}}\left\{\left[-\log(1-e_i^*)\right]^{-c_{GEV}} - 1\right\}, \tag{6}$$

where a_{GEV} (mm/day), b_{GEV} (mm/day), and c_{GEV} (–) denote the location, scale, and shape parameters of the GEV distribution, respectively. The shape parameter, c_{GEV}, controls the skewness of the distribution and enables the fitting of tailed streamflow distributions. The GEV distribution is widely used in the field of hydrology to model floods and drought (extremes) (Katz et al., 2002), as well as the FDC (Booker and Snelder, 2012). If $c_{GEV} = 0$ then the GEV distribution simplifies to the Gumbel distribution.

The lognormal distribution is another statistical distribution that is used widely for the modeling of the FDC [Fennessey and Vogel (1990), among others]. This model can produce the skew necessary to describe the nonsymmetrical shape of the frequency distribution of streamflows. The pseudo-inverse of the lognormal distribution is given by

$$y_i = \exp\left\{a_{LN} - \sqrt{2}b_{LN}\mathrm{erfc}^{-1}\left[2\left(1-e_i^*\right)\right]\right\}, \tag{7}$$

where $\mathrm{erfc}^{-1}(x)$ returns the value of the inverse complementary error function evaluated at x, and a_{LN} (mm/day) and b_{LN} (mm/day) are location and scale coefficients of the lognormal distribution, respectively. A more advanced 3-parameter formulation of the lognormal distribution [see Longobardi and Villani (2013), among

others] provides more flexibility to fit the empirical FDC. The following mathematical formulation defines the pseudo-inverse of this function

$$y_i = c_{LN} + \exp\left\{a_{LN} - \sqrt{2}b_{LN}\mathrm{erfc}^{-1}\left[2(1-e_i^*)\right]\right\}, \quad (8)$$

where c_{LN} (mm/day) constitutes the third parameter of the lognormal distribution. If $c_{LN} = 0$ this function simplifies to the 2-parameter formulation of the lognormal distribution.

We also consider in this study the logistic and generalized Pareto distribution. Their formulations have perhaps not been used widely to describe the empirical FDC, but their usefulness should be verified in the present paper for a meaningful benchmarking of the current state-of-the-art. The logistic distribution (LG) is given by

$$y_i = a_{LG} - b_{LG}\log\left(\frac{1}{1-e_i^*} - 1\right), \quad (9)$$

where a_{LG} (mm/day) and b_{LG} (mm/day) are coefficients of the distribution. The generalized Pareto (GP) distribution is defined as follows

$$y_i = a_{GP} + \frac{b_{GP}}{c_{GP}}\left[(e_i^*)^{-c_{GP}} - 1\right], \quad (10)$$

and the fitting coefficients a_{GP} (mm/day), b_{GP} (mm/day), and c_{GP} (–) need to be derived by fitting against the empirical FDC. This concludes the description of the probabilistic functions (models) of the FDC. These functions use as their main building block the (inverse) CDF of some commonly used probability distribution. In a later section of this paper we will detail how the coefficients in each of these functions are derived. The next section continues our review with nonprobabilistic models of the FDC.

2.3.2. Nonprobabilistic models

The second class of FDC models used in the literature builds on rather standard parametric expressions. These models have in common with their probabilistic counterparts the use of fitting coefficients. These coefficients are subject to inference using some nonlinear minimization method and data of the empirical FDC. The first two nonprobabilistic models involve the logarithmic (LOG) and power (PW) functions

$$y_i = b_{LOG} + a_{LOG}\log(e_i^*), \quad (11)$$

and

$$y_i = b_{PW}(e_i^*)^{-a_{PW}}, \quad (12)$$

where a_{LOG} (mm/day), b_{LOG} (mm/day), a_{PW} (–), and b_{PW} (mm/day) are fitting coefficients. A 2-parameter exponential function was suggested by Quimpo et al. (1983)

$$y_i = a_Q\exp(-b_Q e_i^*), \quad (13)$$

with coefficients a_Q (mm/day) and b_Q (–).

Franchini and Suppo (1996) proposed a 3-parameter expression of the FDC defined as

$$y_i = b_{FS} + a_{FS}(1-e_i^*)^{c_{FS}}, \quad (14)$$

in which a_{FS} (mm/day), b_{FS} (mm/day) and c_{FS} (–) denote the fitting coefficients. This parametric function was originally proposed to describe only the low flow part of the FDC, but has been applied to the entire FDC as well (Sauquet and Catalogne, 2011).

More recently, Viola et al. (2011) proposed a simple 2-parameter function which is given by

$$y_i = \begin{cases} a_V\left(\frac{1}{e_i^*} - 1\right)^{b_V} & \text{if } e_i < 1 - p_0 \\ 0 & \text{if } e_i \geqslant 1 - p_0 \end{cases}, \quad (15)$$

and a_V (mm/day), and b_V (–) are the fitting coefficients. This concludes our description of the nonprobabilistic FDC models.

Practical experience suggests that the probabilistic and nonprobabilistic models discussed thus far are not always flexible enough to fit closely the FDC for a large range of watersheds with contrasting hydrologic behaviors. In the next section we therefore introduce a new class of parametric expressions which are designed specifically to accurately describe the FDCs for a large range of hydrologic behaviors.

2.3.3. Proposed formulations

The functional shape of the FDC has many elements in common with that of the soil water characteristic. This is graphically illustrated in Fig. 3 which plots the water retention function of five different soils presented in van Genuchten (1980). These curves depict the relationship between the volumetric moisture content, θ (x-axis) and the corresponding pressure head, h (y-axis) of a soil and are derived by fitting equation

$$\theta = \theta_r + \frac{\theta_s - \theta_r}{\left[1 + (\alpha|h|)^n\right]^m}, \quad (16)$$

to experimental (θ, h) data collected in the laboratory. This equation is also known as the van Genuchten (VG) model and contains five different coefficients, also called soil hydraulic parameters, where θ_s (cm^3/cm^3) and θ_r (cm^3/cm^3) denote the saturated and residual moisture content, respectively, and α (1/cm), n (–) and m (–) are fitting coefficients that determine the air-entry value and slope of the WRF. In most studies, the value of m is set conveniently to $1 - 1/n$. This not only reduces the number of water retention parameters to four, but also provides a closed-form expression for the unsaturated soil hydraulic conductivity function (van Genuchten, 1980).

The shape of the WRFs plotted in Fig. 3 shows great similarity with the FDCs displayed previously in Fig. 1. This suggests that Eq. (16) might be a good parametric expression to describe the FDC and thus relationship between the exceedance probability of streamflow (x-axis) and its magnitude (y-axis). To make sure that the exceedance probability is bounded exactly between 0 and 1, we set $\theta_r = 0$ and $\theta_s = 1$, respectively. This leads to the following 3-parameter VG formulation of the FDC proposed by Vrugt and Sadegh (2013)

$$e_i^* = \left[1 + (a_{VG}y_i)^{b_{VG}}\right]^{-c_{VG}}, \quad (17)$$

with coefficients a_{VG} (day/mm), b_{VG} (–), and c_{VG} (–). This VG-formulation relates the streamflow (input variable) to its exceedance probability (output variable), and has to be inverted to be consistent with the other formulations used herein. This gives

$$y_i = \frac{1}{a_{VG}}\left[(e_i^*)^{(-1/c_{VG})} - 1\right]^{(1/b_{VG})}. \quad (18)$$

The VG-formulation presented in Eq. (18) can be simplified to a 2-parameter function if we assume that $c_{VG} = 1 - 1/b_{VG}$. We will consider both VG formulations of the FDC.

The VG function is used widely in porous flow models to solve numerically variably saturated water flow. Yet, many other hydraulic models have been proposed in the vadose zone literature to characterize the retention and unsaturated soil hydraulic conductivity functions. We consider herein the lognormal WRF of Kosugi (1994, 1996)

$$e_i^* = \begin{cases} \frac{1}{2}\mathrm{erfc}\left[\frac{1}{\sqrt{2}b_K}\log\left(\frac{y_i - c_K}{a_K - c_K}\right)\right] & \text{if } y_i > c_K \\ 1 & \text{if } y_i \leqslant c_K \end{cases}, \quad (19)$$

where a_K (mm/day), b_K (–) and c_K (mm/day) are coefficients that need to be determined by calibration against the empirical FDC of each watershed. We now need to invert Eq. (19) to get as output the exceedance probability for a given value of the streamflow

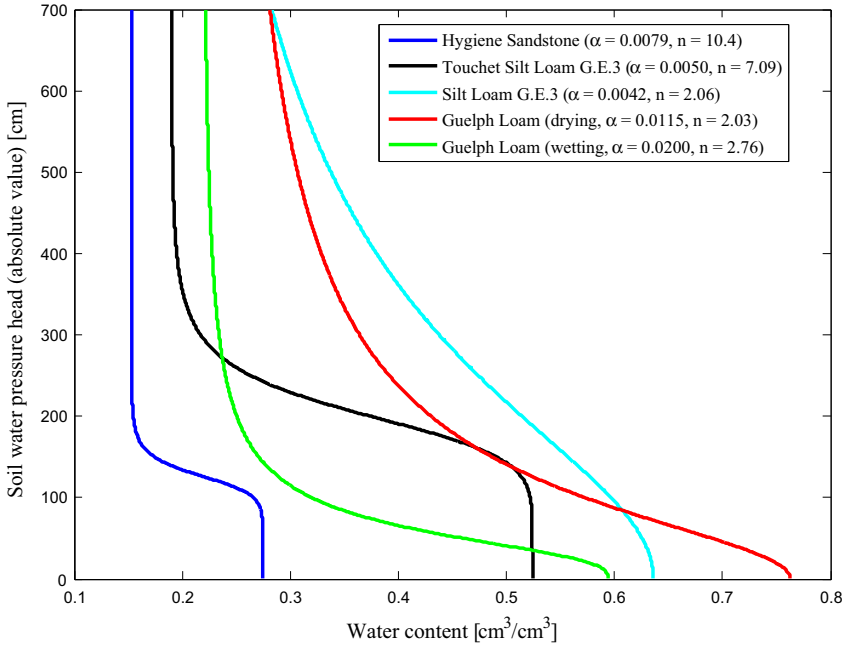

Fig. 3. Water retention functions of five different soil types derived from van Genuchten (1980). The WRF depicts the relationship between the soil water pressure head (cm) and moisture content (cm^3/cm^3). We conveniently plot absolute values of the soil water pressure head (negative in the unsaturated zone).

Table 1
Summary of the probabilistic, nonprobabilistic, and proposed WRF-based FDC models. All these functions return the streamflow value, y_i, for a given value of the exceedance probability, e_i^*. The variables a, b, and c are fitting coefficients whose values need to be derived by calibration against the empirical FDC of a watershed. The acronyms listed in the second column of this table are used in the remainder of this paper to refer to each individual model.

Model name	Acronym	Model formulation
2-parameter formulations		
Lognormal	LN	$y_i = \exp\left\{a_{LN} - \sqrt{2}b_{LN}\text{erfc}^{-1}\left[2(1-e_i^*)\right]\right\}$
Gumbel	G	$y_i = a_G - b_G \log\left[-\log\left(1-e_i^*\right)\right]$
Logistic	LG	$y_i = a_{LG} - b_{LG}\log\left(\frac{1}{1-e_i^*}-1\right)$
Logarithmic	LOG	$y_i = b_{LOG} + a_{LOG}\log(e_i^*)$
Power	PW	$y_i = b_{PW}(e_i^*)^{-a_{PW}}$
Quimpo	Q	$y_i = a_Q \exp\left(-b_Q e_i^*\right)$
Viola	V	$y_i = a_V\left(\frac{1}{e_i^*}-1\right)^{b_V}$
van Genuchten	VG	$y_i = \frac{1}{a_{VG}}\left\{(e_i^*)^{\left[-1/(1-1/b_{VG})\right]}-1\right\}^{\frac{1}{b_{VG}}}$
Kosugi	K	$y_i = a_K \exp\left[\sqrt{2}b_K\text{erfc}^{-1}(2e_i^*)\right]$
3-parameter formulations		
Lognormal	LN	$y_i = c_{LN} + \exp\left\{a_{LN} - \sqrt{2}b_{LN}\text{erfc}^{-1}\left[2(1-e_i^*)\right]\right\}$
Generalized Pareto	GP	$y_i = a_{GP} + \frac{b_{GP}}{c_{GP}}\left[(e_i^*)^{-c_{GP}}-1\right]$
GEV	GEV	$y_i = a_{GEV} + \frac{b_{GEV}}{c_{GEV}}\left\{\left[-\log(1-e_i^*)\right]^{-c_{GEV}}-1\right\}$
Franchini and Suppo	FS	$y_i = b_{FS} + a_{FS}(1-e_i^*)^{c_{FS}}$
van Genuchten	VG	$y_i = \frac{1}{a_{VG}}\left[(e_i^*)^{-1/c_{VG}}-1\right]^{(1/b_{VG})}$
Kosugi	K	$y_i = c_K + (a_K - c_K)\exp\left[\sqrt{2}\,b_K\text{erfc}^{-1}(2e_i^*)\right]$

$$y_i = c_K + (a_K - c_K)\exp\left[\sqrt{2}b_K\text{erfc}^{-1}(2e_i^*)\right]. \quad (20)$$

We can simplify this 3-parameter formulation by setting $c_K = 0$. This 2-parameter formulation of Kosugi is then, after a log-transformation and some rearrangement, equivalent mathematically to the 2-parameter lognormal distribution. The 3-parameter Kosugi model differs however from its counterpart of the lognormal distribution.

The main advantage of the WRF of Kosugi is that its parameters can be related directly to the pore size distribution and hence exhibit a much better physical underpinning than their counterparts of the VG model. This might increase the chances of successful regionalization.

A summary of the different models of the FDC appears in Table 1. The acronym of each model listed in the second column of this table are used in the remainder of this paper when referring to each individual model.

2.4. Change of dependent/independent variables

The functions of the FDC presented in the previous section return the streamflow value (dependent variable) for a given exceedance probability (independent variable), or $y = \mathcal{F}(e)$. For

practical considerations, however it might be useful to have available a direct expression for the exceedance probability instead, and thus $e = \mathcal{F}^{-1}(y)$. This inverse formulation returns the exceedance probability (dependent variable) for a given streamfow value (independent variable) and is particularly useful if one wants to compute (among others) the relative amount of time that the streamflow is likely to exceed a certain target. If this flow value constitutes the maximum capacity of the channel, then the probability of flooding can be assessed. Indeed, this inverse formulation is of great value to decision makers concerned with the design and engineering of dams and other flood protection structures. For example, a structure can be designed to perform well within some range of flows, such as flows that occur between 20% and 80% of the time (or some other selected interval).

The inverse formulation, $e = \mathcal{F}^{-1}(y)$ is rather straightforward to derive for each of the FDC models listed in the previous section. For example, the inverse (= pseudo CDF) of the Gumbel distribution in Eq. (5) can be derived in the following few steps. We first note that $e_i^* = \mathcal{F}^{-1}(y_i)$ and replace the exceedance probability, e_i^* in Eq. (5) with $\mathcal{F}^{-1}(y_i)$. This gives

$$y_i = a_G - b_G \log[-\log(1 - \mathcal{F}^{-1}(y_i))]. \tag{21}$$

We now isolate $\mathcal{F}^{-1}(y_i)$

$$\log[-\log(1 - \mathcal{F}^{-1}(y_i))] = \frac{a_G - y_i}{b_G}, \tag{22}$$

and get rid of the first $\log(\cdot)$ operator at the left hand side using the exponential function

$$-\log(1 - \mathcal{F}^{-1}(y_i)) = \exp\left(\frac{a_G - y_i}{b_G}\right). \tag{23}$$

Table 2
Summary of the probabilistic, nonprobabilistic, and proposed WRF-based FDC models. All these functions return the exceedance probability, e_i^*, for a given value of the streamflow, y_i. The variables $a_.$, $b_.$, and $c_.$ are fitting coefficients whose values need to be derived by calibration against the empirical FDC of a watershed.

Model name	Model formulation
2-parameter formulations	
Lognormal	$e_i^* = 1 - \frac{1}{2}\mathrm{erfc}\left[\frac{a_{LN} - \log(y_i)}{\sqrt{2}b_{LN}}\right]$
Gumbel	$e_i^* = 1 - \exp\left[-\exp\left(\frac{a_G - y_i}{b_G}\right)\right]$
Logistic	$e_i^* = 1 - \left[1 + \exp\left(\frac{a_{LG} - y_i}{b_{LG}}\right)\right]^{-1}$
Quimpo	$e_i^* = -\frac{1}{b_Q}\log\left(\frac{y_i}{a_Q}\right)$
Viola	$e_i^* = \left[\left(\frac{y_i}{a_V}\right)^{(1/b_V)} + 1\right]^{-1}$
Logarithmic	$e_i^* = \exp\left(\frac{y_i - b_{LOG}}{a_{LOG}}\right)$
Power	$e_i^* = \left(\frac{y_i}{b_{PW}}\right)^{(-1/a_{PW})}$
VG	$e_i^* = \left[1 + (a_{VG}y_i)^{b_{VG}}\right]^{(1/b_{VG}-1)}$
Kosugi	$e_i^* = \frac{1}{2}\mathrm{erfc}\left[\frac{1}{\sqrt{2}b_K}\log\left(\frac{y_i}{a_K}\right)\right]$
3-parameter formulations	
Lognormal	$e_i^* = 1 - \frac{1}{2}\mathrm{erfc}\left[\frac{a_{LN} - \log(y_i - c_{LN})}{\sqrt{2}b_{LN}}\right]$
Generalized Pareto	$e_i^* = \left[1 + \frac{c_{GP}(y_i - a_{GP})}{b_{GP}}\right]^{(-1/c_{GP})}$
GEV	$e_i^* = 1 - \exp\left\{-\left[1 + c_{GEV}\left(\frac{y_i - a_{GEV}}{b_{GEV}}\right)\right]^{(-1/c_{GEV})}\right\}$
Franchini and Suppo	$e_i^* = 1 - \left(\frac{y_i - b_{FS}}{a_{FS}}\right)^{1/c_{FS}}$
VG	$e_i^* = \left[1 + (a_{VG}y_i)^{b_{VG}}\right]^{-c_{VG}}$
Kosugi	$e_i^* = \frac{1}{2}\mathrm{erfc}\left[\frac{1}{\sqrt{2}b_K}\log\left(\frac{y_i - c_K}{a_K - c_K}\right)\right]$

If we repeat the same operation, and rearrange the final equation we derive

$$e_i^* = \mathcal{F}^{-1}(y_i) = 1 - \exp\left[-\exp\left(\frac{a_G - y_i}{b_G}\right)\right]. \tag{24}$$

These steps can be repeated for each of the parametric expressions of the FDC in the previous Section 2.3.

Table 2 lists for each FDC model of Section 2.3 (see also Table 1) the inverse function, $\mathcal{F}^{-1}(y_i)$. We do not summarize conditions for the values of the parameters in each FDC function. Their values are carefully chosen to avoid division by zero (example: $b_{LN} > 0$) and ensure that each log operator has strictly positive input arguments (example: $a_Q > 0$).

2.5. Parameter estimation of FDC models

Now we have discussed the different FDC models we are left with inference of their coefficients. We have developed a MATLAB program called "FDCFIT" which automatically determines the best values of the fitting coefficients of the FDC models used herein for a given streamflow data record. Graphical output is provided as well. We consider two different calibration cases involving optimization of the FDC coefficients in the (a) streamflow, **Y**-space, and (b) exceedance probability, **E**-space using a standard sum of squared error (SSE) objective function

$$\mathrm{SSE}(\mathbf{x}|\hat{\mathbf{E}}) = \sum_{i=1}^{n}[\hat{y}_i - \mathcal{F}(\mathbf{x}|\hat{e}_i)]^2 \quad \text{in } \mathbf{Y}\text{-space} \tag{25}$$

$$\mathrm{SSE}(\mathbf{x}|\hat{\mathbf{Y}}) = \sum_{i=1}^{n}\left[\hat{e}_i - \mathcal{F}^{-1}(\mathbf{x}|\hat{y}_i)\right]^2 \quad \text{in } \mathbf{E}\text{-space} \tag{26}$$

where $\mathbf{x} = \{a_., b_.\}$ or $\{a_., b_., c_.\}$ is the m-vector of fitting coefficients, $\hat{\mathbf{E}} = \{\hat{e}_1, \ldots, \hat{e}_n\}$ and $\hat{\mathbf{Y}} = \{\hat{y}_1, \ldots, \hat{y}_n\}$ denote the measured values of the exceedance probability and streamflow, respectively, and $\mathcal{F}(\cdot)$ and $\mathcal{F}^{-1}(\cdot)$ signify the formulations of the FDC model in the streamflow (Table 1) and exceedance probability (Table 2) space.

We consider separately these two different calibration cases as they lead to quite different optimized values of the coefficients of each FDC model. Calibration in the **Y**-space emphasizes fitting of the peak flows at low exceedance probabilities. The sensitivity to lower flows can be increased if a ℓ^1-type objective function were implemented using the absolute rather than squared values of the streamflow error residuals. Calibration in the **E**-space places equal importance to each observation of the exceedance probability, and therefore should lead to a model fit that describes nicely the entire FDC. In the results section we will discuss the results of both calibration cases.

The calibration of each FDC model demonstrated to be a much more difficult task than initially expected. In fact, a reasonable conjecture is that FDC functions and their optimized parameters presented in the literature might have been spurious and subject to premature convergence. A suite of different optimization algorithms were used and tested to estimate the optimal values of the coefficients of each FDC model and watershed. None of these methods were always able to find successfully the global minimum. This is a rather surprising finding given the rather low dimensionality of the parameter space. Response surfaces of the FDC models revealed the culprit. For some of the watersheds the response surfaces were rather flat and the global minimum of Eqs. (25/26) well hidden in a small pocket of the parameter space.

After comprehensive testing of different optimization algorithms, we implemented in the program FDCFIT a multi-start gradient-based local optimization approach with Levenberg Marquardt (LM) (Marquardt, 1963). A total of 20 LM trials were used

Table 3
Performance statistics of the quality of fit of each individual FDC model. We list the mean and standard deviation of the Root Mean Square Error (RMSE) (mm/day) derived from Eqs. (25/26), and the percentage of watersheds each respective 2, or 3-parameter model provides the best fit to the empirical FDCs. The values listed between parenthesis signify the results when the models are calibrated in the exceedance probability or **E**-space.

Model name	Mean RMSE	STD of RMSE	% Best model
2-parameter formulations			
Lognormal	0.2864 (0.0205)	0.1975 (0.0134)	65.02 (43.02)
Gumbel	0.9666 (0.0611)	0.6488 (0.0197)	0.70 (0.93)
Logistic	1.2228 (0.0768)	0.7741 (0.0176)	0 (0)
Quimpo	0.7983 (0.0650)	0.5656 (0.0252)	0.23 (0.23)
Viola	0.5948 (0.0211)	0.3900 (0.0130)	3.72 (14.65)
Logarithmic	0.7516 (0.0410)	0.5579 (0.0189)	4.15 (6.28)
Power	0.7848 (0.0973)	0.5017 (0.0343)	0.70 (2.33)
VG	0.4361 (0.0276)	0.3154 (0.0149)	25.48 (31.63)
Kosugi	0.2864 (0.0205)	0.1975 (0.0134)	65.02 (43.02)
3-parameter formulations			
Lognormal	0.2370 (0.0126)	0.1701 (0.0099)	23.95 (18.37)
Generalized Pareto	0.2697 (0.0138)	0.2007 (0.0080)	9.53 (22.33)
GEV	0.3512 (0.0158)	0.2393 (0.0114)	1.86 (8.84)
Franchini and Suppo	0.6989 (0.0722)	0.5023 (0.0174)	1.40 (0.23)
VG	0.1747 (0.0137)	0.1313 (0.0073)	63.26 (26.98)
Kosugi	0.2370 (0.0119)	0.1701 (0.0071)	23.95 (23.25)

to locate the global minimum of the fitting coefficients of each model and watershed. These trials were initialized at different starting points drawn randomly from the prior parameter space with Latin hypercube sampling (McKay et al., 1979). In case that the LM method was unable to reduce substantially the SSE the (derivative-free) Nelder-Mead Simplex algorithm (Nelder and Mead, 1965) was used instead to minimize Eqs. (25/26). This hybrid two-step approach demonstrated to be robust and CPU-efficient.

In a separate trial with DREAM (Vrugt et al., 2008, 2009) we also determined for each watershed the posterior uncertainty of each of the coefficients of the FDC models. A standard Gaussian (least-squares type) likelihood function was used in all these calculations with default settings of the algorithmic variables of DREAM. Convergence of the chains to a limiting distribution was assessed with different diagnostics (Vrugt, 2016).

3. Results and discussion

Table 3 summarizes the performance of each of the FDC models for the MOPEX data set used herein. We list separately the first (mean) and second-order (standard deviation) moment of the Root Mean Square Error (RMSE) of the fit to the empirical FDCs of the 430 different watersheds. Performance statistics are presented for both calibration cases in the streamflow and exceedance probability space (between parenthesis). For model selection purposes we also list the number of times (expressed in %) each respective FDC model achieves the lowest RMSE among its constituent formulations with similar structural complexity (number of parameters). Note, we do not consider herein metrics such as Akaike's and Bayes' information criterion as the number of data points of the FDC is much larger than the number of parameters of each model. Hence, the RMSE suffices as metric for model selection.

The results in Table 3 highlight several key findings. First, the proposed 2-parameter FDC models of K and VG provide substantially lower mean RMSE values than their counterparts with similar structural complexity used in the hydrologic literature. From all 2-parameter models, the K model is preferred receiving the best performance in the streamflow space for about 65% of the watersheds, and for 43% of the basins in the exceedance probability space. The VG model is ranked second with best performance for more than 25% of watersheds in the **Y**-space and 31% in the **E**-space. Second, the 2-parameter K model exhibits, as expected, the same performance as the 2-parameter LN model. Third, the Q and LG models fit the empirical FDCs rather poorly in both the **Y**- and **E**-spaces. Fourth, among the 3-parameter formulations of the FDC, the VG model generally exhibits the best performance with lowest RMSE for about 63% of the watersheds when evaluated in the **Y**-space and 27% of basins when calibrated in the **E**-space. Fifth, the 3-parameter K and LN models, although dissimilar in their mathematical formulations, give identical results in the **Y**-space yet different RMSE values in the exceedance probability space. This apparent discrepancy can be explained by further analysis of the models and fitting results. Both models are structurally similar at low exceedance probabilities (high flows), and this part of the curve determines the coefficients of the FDC models when fitting in the streamflow space. The differences between these two models are better reflected when they are calibrated in the exceedance probability space, and all flow observations are treated equally. Sixth, the 3-parameter FS model provides a rather poor fit to the data with RMSE of 0.6989 (mm/day) which is even inferior to some of the 2-parameter FDC models. For all intents and purposes the 3-parameter formulation of the VG model achieves the best overall results. This model is thus preferred if the fitting of the empirical FDC is of main concern.

We have considered bimodal formulations of the VG and K models as well (Durner, 1994). These 5-parameter models were constructed by a linear superposition of two of their 2-parameter formulations and include an additional weight for both (sub) curves. These bimodal FDC formulations are superior to the models used herein when evaluated in the **E**-space, but showed no improvement in the **Y**-space. For two reasons, we decided not to include these 5-parameter formulations in the present paper. First, bimodal formulations of the WRF cannot be inverted analytically. This complicated their evaluation in the streamflow space. Second, the parameters of these models exhibit rather poor regionalization relationships (as will be shown later).

To provide more insights into the fitting results for individual catchments, consider Fig. 4 that plots histograms of the RMSE (mm/day) values of the 430 different watersheds. Color coding is used to differentiate among the FDC models. To simplify visual interpretation a common x-axis was used for all different models and complexities. The results presented in this figure confirm our earlier conclusions that the proposed WRF-based models (and 2-parameter LN model) are superior to their counterparts used in the literature. For the 2-parameter FDC models, the LN (plot A) and K (Plot E) models are preferred as their distribution of RMSE values is most skewed to the left in direction of zero RMSE. The 2-parameter VG model (plot I) provides a RMSE distribution that is very similar to that of the K model but with somewhat larger mean value. For the 3-parameter models, the VG model receives the best results with mode of the RMSE histogram closest to zero and relatively little dispersion around this value. This plot confirms our previous finding that the VG-3 model outperforms all other models and should be used if the purpose of application is to predict the streamflow for a given exceedance probability. The 3-parameter K (plot N) and LN (plot M) models provide very similar RMSE distributions, which are in close agreement as well with the marginal distribution of the GP model (plot F). From all 3-parameter models, the performance of the FS model (plot K) is rather poor with mode of the RMSE distribution of about 0.8 (mm/day) and values that range between 0 and 3 (mm/day).

Thus far we have focused our attention on the quality of fit of the individual FDC models without recourse to assessment of their parameter sensitivity, identifiability and correlation. Fig. 5 plots, for a large range of exceedance probabilities, the sensitivity of the simulated streamflow values to each of the individual parameters in the VG (top panel) and K (bottom panel) models.

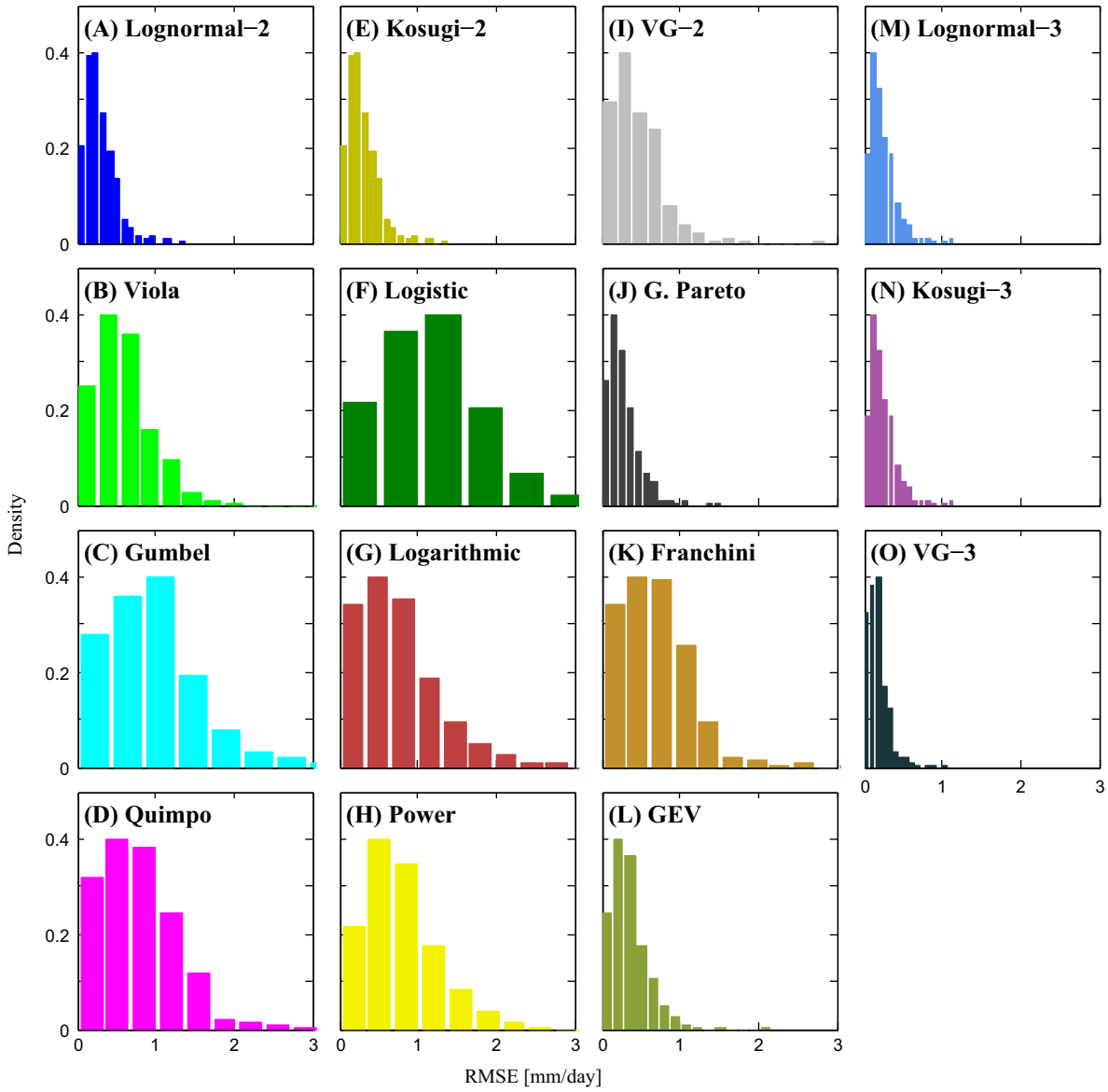

Fig. 4. Histogram of the RMSE (mm/day) values of the 430 MOPEX watersheds.

Color coding is used to differentiate among the different parameters of each model. We display separately the results for the 2 (left column), and 3 (right column) parameter formulations of both models. We follow Vrugt et al. (2002) and derive these partial sensitivities, $\partial y_i/\partial x_j$ analytically by differentiation of the VG and K models to each of their m coefficients, $j = \{1, \ldots, m\}$. For example, for the 2-parameter formulation of K, the m-vector of parameters is $\mathbf{x} = \{a_K, b_K\}$, and their partial sensitivities are given by

$$\begin{aligned} \partial y_i/\partial a_K &= \exp\left[\sqrt{2}\, b_K\, \mathrm{erfc}^{-1}(2\, e_i^*)\right], \\ \partial y_i/\partial b_K &= \sqrt{2}\, a_K \mathrm{erfc}^{-1}(2\, e_i^*)\, \exp\left[\sqrt{2}\, b_K \mathrm{erfc}^{-1}(2\, e_i^*)\right], \end{aligned} \tag{27}$$

and their numerical values are plotted in Fig. 5B with a blue and red line, respectively using representative values of a_K and b_K, and 1000 values of the exceedance probability using equidistant intervals between 0 and 1. We draw the following conclusions based on the results presented in Fig. 5.

In the first place, the parameters of the 2-parameter VG and K models appear to be most sensitive at high flows and exhibit almost negligible sensitivity at large values of the exceedance probability. In other words, if these models are calibrated in the streamflow space then their coefficients are determined primarily from data of the rainfall-driven part of the hydrograph. Second, the 3-parameter VG and K models exhibit a higher sensitivity than their 2-parameter formulations at lower streamflows. This is particularly true for the VG model and should simplify inference. Third, the 3-parameter VG model appears to be most sensitive to each of its parameters with values of the $\partial y_i/\partial c_{VG}$ that are, on average, highest of all the four proposed parametric expressions. Thus if parameter uncertainty is of main concern then the 3-parameter formulation of VG is preferred as its fitting coefficients are most sensitive and thus best defined by the empirical FDC. Finally, all of the parameters in each of the models show their maximum sensitivity at approximately similar streamflow values. This finding is rather unfortunate as it makes all four FDC-models vulnerable to parameter correlation (interaction). This is not particularly desirable if the fitting coefficients are used as summary statistics for diagnostic model evaluation.

We now provide a more detailed visual comparison of the observed and fitted FDCs. We select, from the MOPEX data set, three watersheds with widely different rainfall-runoff response

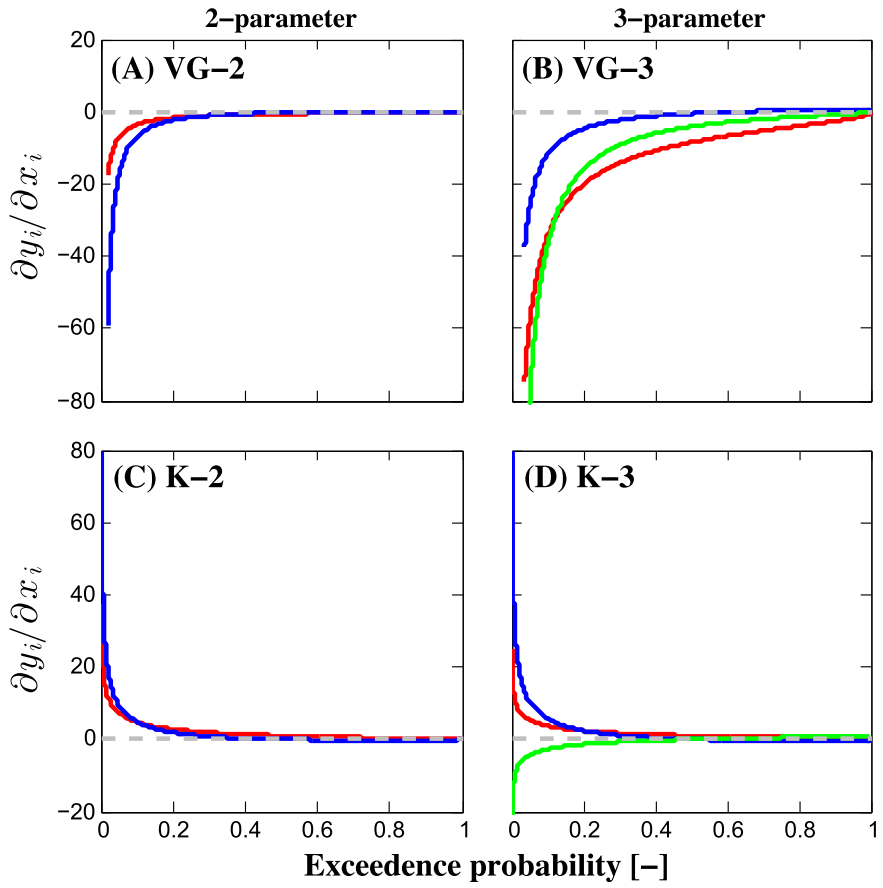

Fig. 5. Partial parameter sensitivities of the VG (top panel) and K (bottom panel) models of the FDC for a range of different streamflow values. Color coding is used to differentiate between the parameters *a.* (red), *b.* (blue), and *c.* (green) of the VG-2, VG-3, K-2, and K-3 models. The gray dashed line plots zero sensitivity. (For interpretation of the references to color in this figure legend, the reader is referred to the web version of this article.)

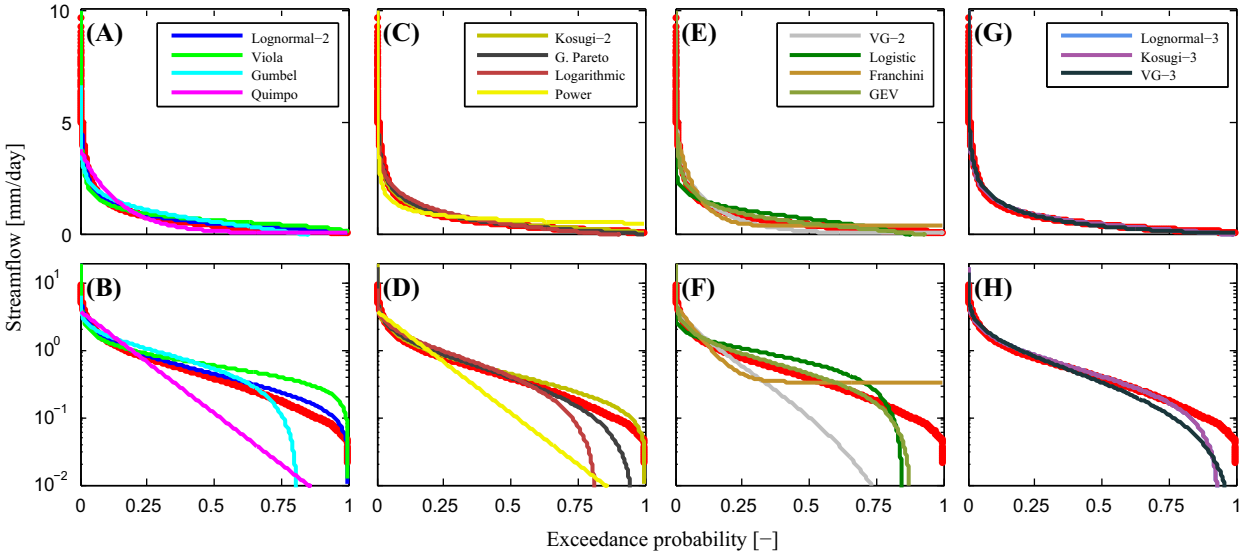

Fig. 6. Comparison of the empirical (red dots) and fitted FDCs of the Green river watershed near Genesco, IL, USA. The different models of Tables 1 and 2 are color coded. The top panel (A, C, E, G) uses an arithmetic (linear) scale of the streamflow values, whereas the bottom panel (B, D, F, H) uses a logarithmic scale. (For interpretation of the references to color in this figure legend, the reader is referred to the web version of this article.)

and present their empirical FDCs in Figs. 6 (Green river), 7 (Kankakee river), and 8 (Little river). The fit of each model is color coded and derived by calibration in the streamflow space using the objective function of Eq. (25). To help illuminate differences between the fit of the fifteen FDC models, we use an arithmetic (top) and logarithmic (bottom) scale of the streamflow values. The log scale makes it easier to compare the values of the streamflow that cover a relatively large range. The empirical FDC is separately indicated using the red dots. Four different graphs are used for each watershed to simplify graphical interpretation.

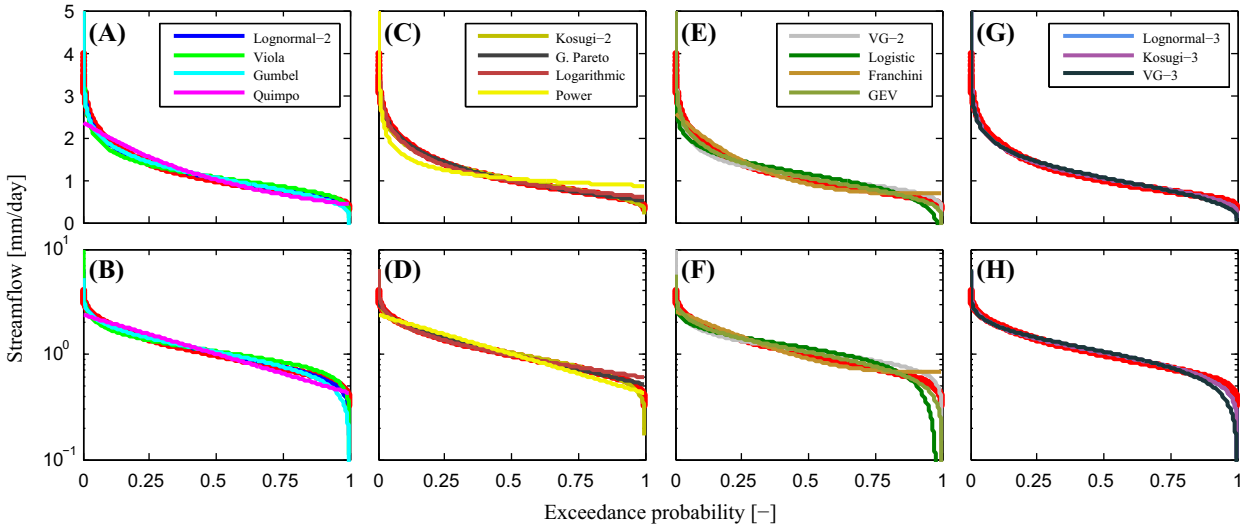

Fig. 7. Comparison of the empirical (red dots) and fitted FDCs of the Kankakee river, IN, USA. The different models of Tables 1 and 2 are color coded. The top panel (A, C, E, G) uses an arithmetic (linear) scale of the streamflow values, whereas the bottom panel (B, D, F, H) uses a logarithmic scale. (For interpretation of the references to color in this figure legend, the reader is referred to the web version of this article.)

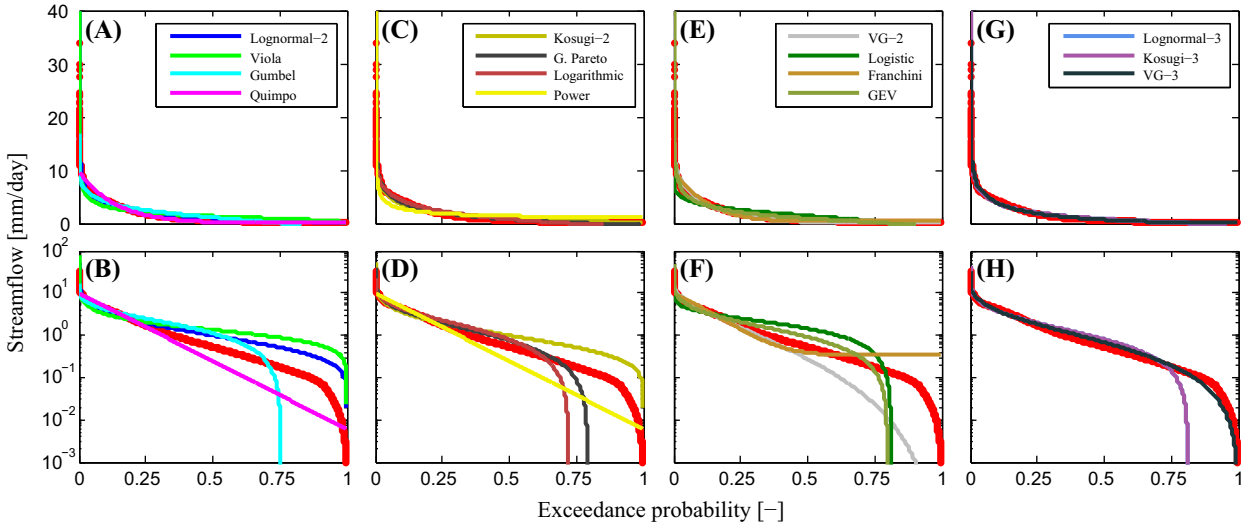

Fig. 8. Comparison of the empirical (red dots) and fitted FDCs of the Little river near Horatio, AR, USA. The different models of Tables 1 and 2 are color coded. The top panel (A, C, E, G) uses an arithmetic (linear) scale of the streamflow values, whereas the bottom panel (B, D, F, H) uses a logarithmic scale. (For interpretation of the references to color in this figure legend, the reader is referred to the web version of this article.)

Table 4
Mean values of the correlation coefficients of the DREAM-derived posterior parameter samples for the 430 different watersheds of the MOPEX data set. Values that are listed in parenthesis pertain to calibration in the **E**-space instead.

	a_{VG}	b_{VG}		a_K	b_K
2-parameter formulations					
a_{VG}	1.00	0.90 (0.81)	a_K	1.00	0.89 (0.16)
b_{VG}	0.90 (0.81)	1.00	b_K	0.89 (0.16)	1.00

	a_{VG}	b_{VG}	c_{VG}	a_K	b_K	c_K
3-parameter formulations						
a_{VG}	1.00	0.15 (0.89)	0.64 (0.96)	a_K	1.00	0.90 (0.44)	0.93 (0.46)
b_{VG}	0.15 (0.89)	1.00	0.71 (0.93)	b_K	0.90 (0.44)	1.00	0.91 (0.67)
c_{VG}	0.64 (0.96)	0.71 (0.93)	1.00	c_K	0.93 (0.46)	0.91 (0.67)	1.00

The empirical FDCs plotted in Figs. 6–8 exhibit their well-known hyperbolic shape when plotted using a linear scale of the streamflow observations. The FDCs of the Green river and Little river appear somewhat similar, although their range of flows differs somewhat. For the Kankakee watershed a tail is visible at the extreme lower end of the FDC with lowest streamflow values. Such tailing behavior is often observed in the WRF of soils and signifies the air-entry value. The characteristic "S"-shape of the empirical FDCs is most apparent when a log-scale is used for the streamflow data.

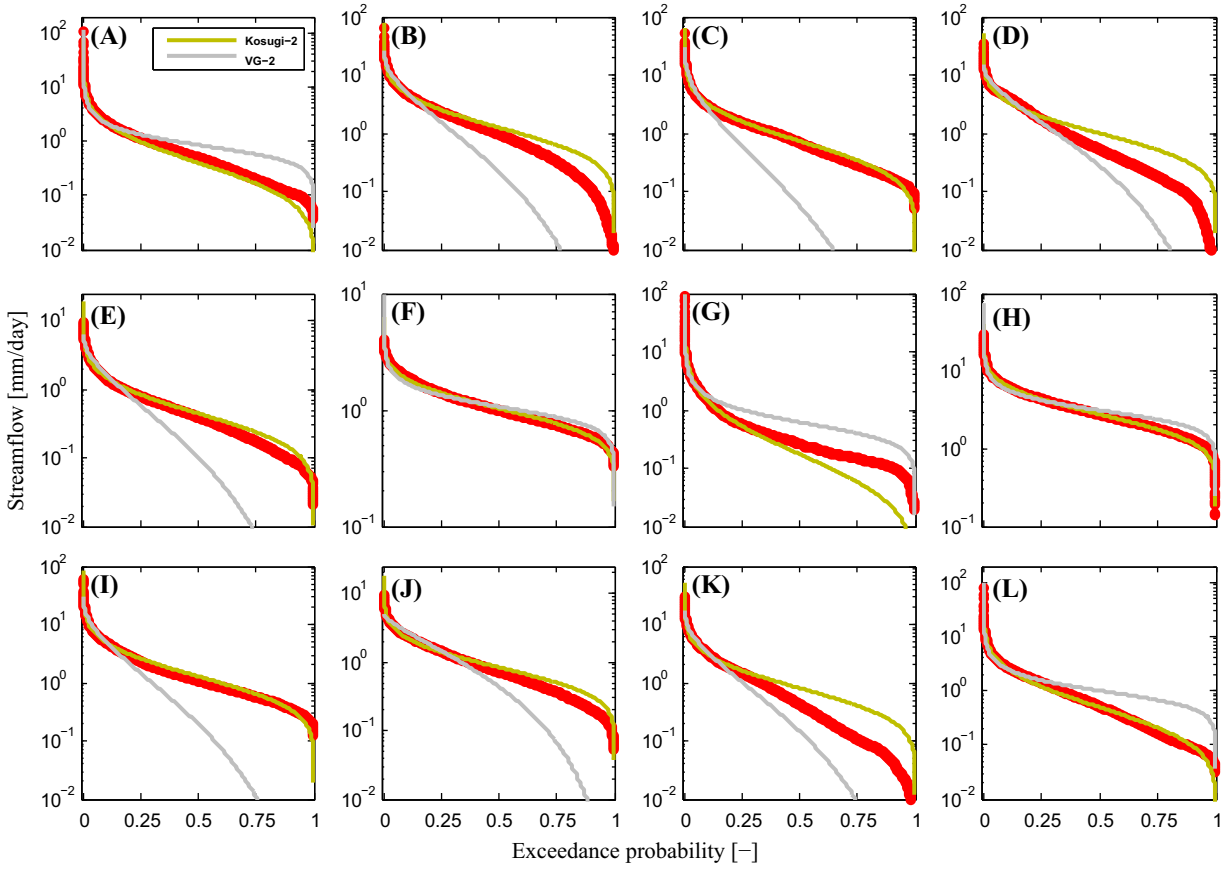

Fig. 9. Comparison of the simulated FDCs of the 2-parameter VG and K models against their empirical counterparts (red dots) of the MOPEX data set. Each model was calibrated in the streamflow space by minimization of Eq. (25) using a multi-start Levenberg–Marquardt approach. The different graphs correspond to the (A) SB Potomac, (B) Tygart Valley, (C) NF Holston, (D) Little, (E) Green, (F) Kankakee, (G) EF San Gabriel, (H) White, (I) Pemigewasset, (J) Little Pee Dee, (K) Licking, and (L) Genesee river basins, respectively. (For interpretation of the references to color in this figure legend, the reader is referred to the web version of this article.)

Visual analysis of the behavior of each model demonstrates that it is particularly difficult to judge their quality of fit if a linear scale of the streamflow observations is used. In fact, all models appear to describe the empirical FDCs reasonably well, and the observed $\{\hat{e}_i^*, \hat{y}_i\}$ data pairs are hardly visible. The differences between the models become most apparent when the FDCs are plotted on a logarithmic streamflow scale. The 3-parameter formulation of VG is most supported by the data as it provides the closest fit to the empirical FDCs. The 3-parameter LN and K models receive an almost similar performance, yet some deviations of these models are apparent at low flows (high exceedance probabilities), particularly for the Little river watershed. These findings are supported by our previous results listed in Table 3.

If a 2-parameter formulation of the FDC is preferred then the K model (and thus LN distribution) exhibits superior performance. The 2-parameter VG model does a good job in fitting the FDCs of the MOPEX watersheds, yet this model systematically underestimates the exceedance probabilities of the lower streamflow values. This mismatch is particularly noticeable for the Green river and Little river (Figs. 6 and 8) and highlights a structural deficiency of the VG-2 model for watersheds with a relatively large number of low flows.

The benefits of using a more complex FDC model are most spectacular for the VG model and Little river. The 3-parameter formulation of this model achieves a much better performance than its 2-parameter counterpart. This VG-2 model cannot describe adequately the discharge of this watershed which falls rapidly from about 35 to 7 mm/day, then decreases linearly to about 2 mm/day, and then smoothly reduces to values of zero.

The results presented in Figs. 6–8 display relatively large deficiencies between the empirical and simulated FDCs at intermediate and low flows. This is particularly true for the 2-parameter models. This mismatch can be remedied considerably if the FDC models are calibrated in the exceedance probability space, results of which have been summarized in Table 3. This issue of how to calibrate FDC models has received little attention in the hydrologic literature, but is of imminent importance in their application. What is more, some FDC models predict negative values of the streamflow when their formulations of Table 1 are evaluated at higher values of the exceedance probability. Examples include the 2-parameter G, LG, and LOG, and the 3-parameter GEV model. What is more, the 3-parameter GP, LN, and K models also allow for negative streamflow prediction, if their third parameter, c, is permitted to adopt negative values in the optimization process. Thus, some care should be exercised with their use and evaluation. The other models are not affected by this behavior, for instance, the exceedance probabilities and streamflow values predicted by the K and VG models are bounded between $[0-1]$, and $[0-\infty]$, respectively.

We now proceed with an in-depth study of the interaction between the parameters of the WRF-based FDC formulations. Table 4 lists average linear correlation coefficients of the fitting coefficients of the VG and K models derived from Markov chain Monte Carlo (MCMC) simulation with DREAM using the 430 different watersheds of the MOPEX data set. These values are calculated by computing the mean of the absolute values of the linear correlation coefficients among the posterior parameter samples of each individual watershed. Absolute values have to be used for each

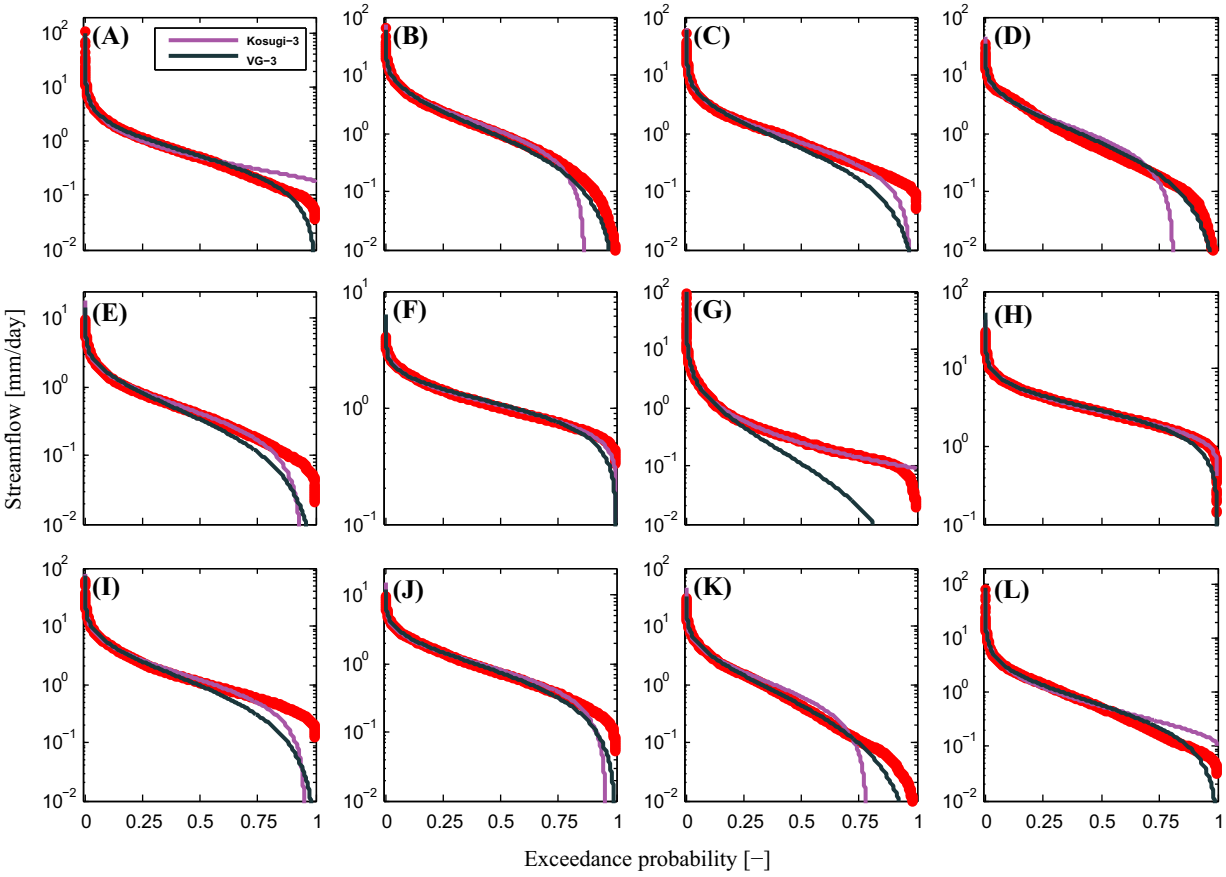

Fig. 10. Comparison of the simulated FDCs of the 3-parameter VG and K models against their empirical counterparts (red dots) of the MOPEX data set. Each model was calibrated in the streamflow space by minimization of Eq. (25) using a multi-start Levenberg–Marquardt approach. The different graphs correspond to the (A) SB Potomac, (B) Tygart Valley, (C) NF Holston, (D) Little, (E) Green, (F) Kankakee, (G) EF San Gabriel, (H) White, (I) Pemigewasset, (J) Little Pee Dee, (K) Licking, and (L) Genesee river basins, respectively. (For interpretation of the references to color in this figure legend, the reader is referred to the web version of this article.)

watershed to avoid cancellation of positive and negative correlations. Of course, strong parameter correlation is not of much importance if quality of fit is the main concern in application of the VG and K models, but becomes particularly important if the fitting coefficients of each model are used as summary metrics for diagnostic analysis. Independent model parameters are also desired for regionalization studies when relating model parameters to one or more basin characteristics.

The results presented in Table 4 illustrate several important findings. First, the parameters of the VG-2 model exhibit a much stronger posterior correlation than the coefficients of the VG-3 model when calibrated against streamflow data. This result is perhaps rather unexpected but in part explained by the much improved fit of the 3-parameter formulation of this model. The posterior correlations of both VG model formulations are more similar when calibrated in the exceedance probability space. Second, the posterior correlation of the K-3 model are somewhat larger than those derived for the K-2 model. This is true for both calibration cases. Third, the 2-parameter formulations of the K and VG models exhibit a similar correlation when calibrated in the streamflow space. If these models are fitted against the exceedance probabilities, then the K model is preferred as its coefficients exhibit a much smaller correlation. Fourth, the posterior parameter correlations of the VG-3 model are much lower than their counterparts of the K-3 model when fitted against the streamflow data of the FDC. The opposite result is true if both models are calibrated against the exceedance probabilities.

These results might be somewhat confusing to interpret. Main results are that the two calibration cases lead to (very) different correlation structures among the parameters of the VG and K models, and that the VG-3 model exhibits much lower parameter interdependencies than the K-3 model when calibrated in the streamflow space. This latter finding is supported by the behavior of the partial derivatives of the parameters (see Fig. 5) which have a larger sensitivity in the VG-3 model. The opposite conclusion about these sensitivities is true when the VG-3 and K-3 models are fitted against the exceedance probability.

We now present in Figs. 9 and 10 the fitting results of the proposed 2-parameter and 3-parameter VG and K parametric expressions of the FDC for a sample of 12 different watersheds distributed over the USA. This includes the (A) SB Potomac (B) Tygart Valley (C) NF Holston (D) Little (E) Green (F) Kankakee (G) EF San Gabriel (H) White (I) Pemigewasset (J) Little Pee Dee (K) Licking, and (L) Genesee, river basins in the states of West Virginia, West Virginia, Virginia, Arkansas, Illinois, Indiana, California, Washington, New Hampshire, South Carolina, Kentucky, and Washington, respectively.

Comparison of the fitting results of Figs. 9 and 10 demonstrates an improved skill of the 3-parameter formulations of VG and K over their 2-parameter formulations. This enhanced fit might not always be readily apparent as the models have been calibrated in the **Y**-space and thus favor fitting the "left" end of the empirical FDC with the highest streamflow values. The improvement in fit of the VG-3 model over its two-parameter formulation is

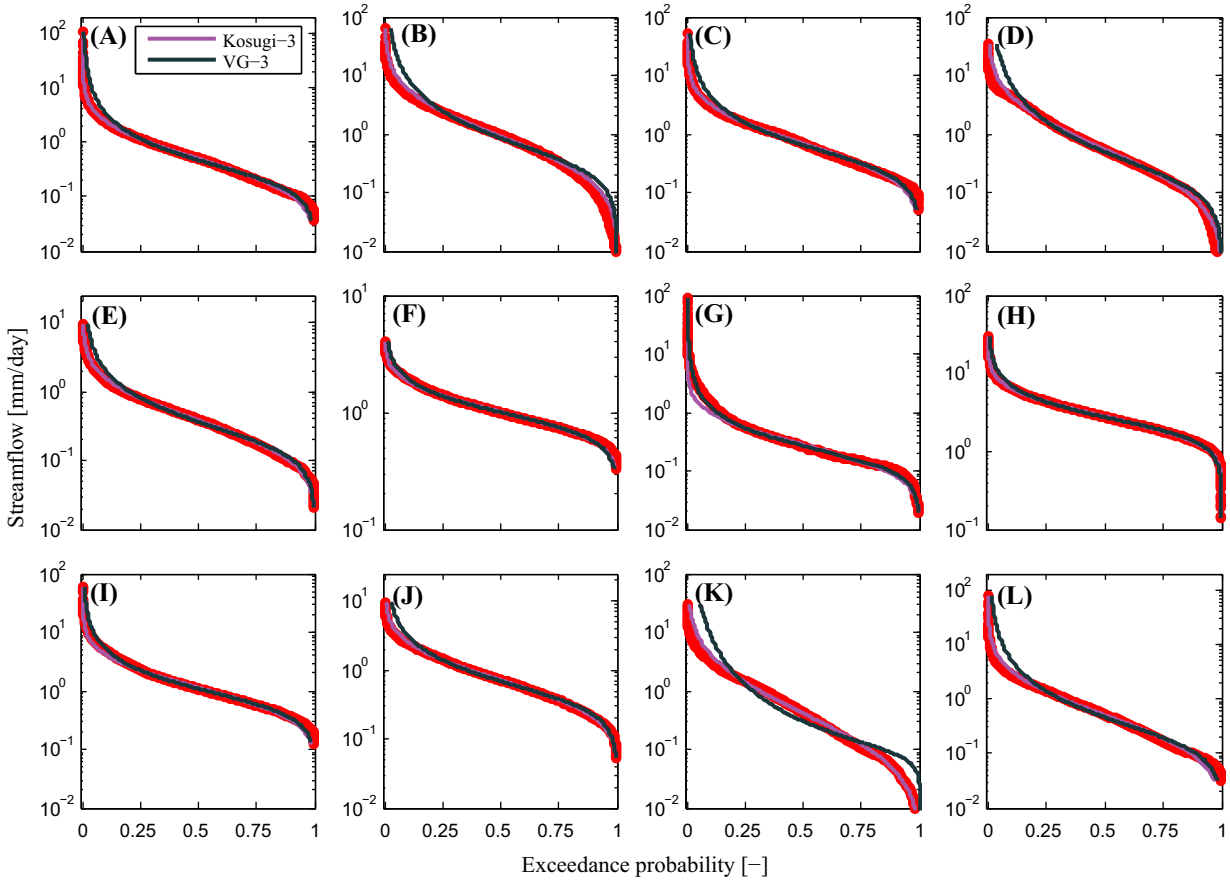

Fig. 11. Comparison of the simulated FDCs of the 3-parameter VG and K models against their empirical counterparts (red dots) of the MOPEX data set. Each model was calibrated in the exceedance probability space by minimization of Eq. (26) using a multi-start Levenberg–Marquardt approach. The different graphs correspond to the (A) SB Potomac, (B) Tygart Valley, (C) NF Holston, (D) Little, (E) Green, (F) Kankakee, (G) EF San Gabriel, (H) White, (I) Pemigewasset, (J) Little Pee Dee, (K) Licking, and (L) Genesee river basins, respectively. (For interpretation of the references to color in this figure legend, the reader is referred to the web version of this article.)

significant. The added skill provided by the third parameter in the K model is not as convincing, because the K-2 model does a much better job than the VG-2 model in reproducing the empirical FDCs. This might not be immediately visible in performance metrics such as the RMSE as this statistic is determined in large part by deviations in the large flows. Indeed, the use of a log-scale for the streamflow values exaggerates the differences between the modeled and measured FDC for lower flow values. Indeed, the difference on a log-scale could equate to one order of magnitude whereas the difference between the empirical and fitted FDC is only 0.1 mm/day, or 0.001 mm/day for that matter. This hardly influences metrics such as the RMSE.

Some persistent deviations of the 2-parameter K and VG models remain apparent at the low flows (high exceedance probabilities), particularly for semi-arid and arid watersheds that are characterized by long dry periods and occasional but large precipitation events (convective thunderstorms). The 3-parameter formulation of VG improves the fitting of the FDC of such watersheds, but cannot reproduce the two distinctly different processes of runoff generation. A bimodal formulation of the K and VG model will improve significantly the description of the FDC of semi arid and arid watersheds, in large part because of their ability to describe separately the low and high flow portions of the FDC. These models are not considered herein for reasons discussed before.

Fig. 11 plots the results of the 3-parameter K and VG models for the 12 different watersheds of Fig. 10, but now calibrated in the exceedance probability, **E**-, space rather than the streamflow, **Y**-, space. While the fit to the lower end of the curve has improved in all presented watersheds, model performance for high flows of some watersheds has deteriorated somewhat. This is most visible for the Licking and Genesee river basins plotted in graphs K and L, respectively. Calibration in the **E**-space places equal weight on each FDC-data point and therefore should lead to a model fit that mimics as closely as possible the entire range of flows of the FDC.

Our results demonstrate that the easiest watersheds to fit are those that are relatively wet and in which the baseflow from the groundwater reservoir makes up a large portion of the total streamflow. The FDC then exhibits a relatively mild slope with two clearly defined tails. Such "S"-shaped curve is easiest to capture with the 2- and 3-parameter formulations of VG and K. Examples includes the Kankakee (F), White (H), and Little Pee Dee (J) river basins.

We conclude the results section with some remarks: (1) The fitting of the proposed FDC models is not without problems. We therefore recommend to use different starting points with a local search method to minimize chances of premature convergence to the wrong values of the FDC fitting coefficients and (2) The proposed WRF-based functions demonstrate low sensitivity to low flows (Fig. 5), and hence some care should be exercised if these models are used to estimate the exceedance probability of extreme events. One way to mitigate this problem is to calibrate these models in the **E**-space using the formulations of the models of Table 2. The results of this approach have been presented in Table 3 and favor the use of the VG-3 model. Alternatively, one could use a ℓ^1 formulation of the objective function to weight all streamflow observations equally.

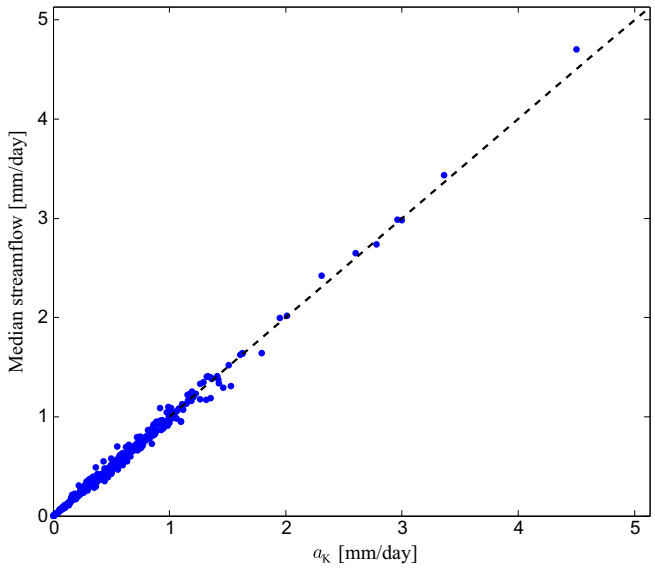

Fig. 12. Scatter plot of the optimized value of parameter a_K of the K-2 model and the median streamflow value. Each dot represents a different watershed of the MOPEX data set. The dashed black line signifies the 1:1 line.

4. Regionalization of FDC models

If the main interest in application of FDC models is to fit the empirical FDC then the VG-3 model is preferred. This model achieves the best performance for the watersheds of the MOPEX data set. The fitted model can then be used to calculate the exceedance probability for a given flow level, or vice versa the flow associated with a certain exceedance probability. All this is useful for decision makers considered with flood-risk management. Moreover, the parametric expressions proposed herein are also of great use in diagnostic model evaluation (Vrugt and Sadegh, 2013) to help find behavioral model simulations that honor the empirical FDC as closely and consistently as possible. The optimized values of the coefficients are then used as summary metrics.

We now investigate whether we can relate the optimized coefficients of each model to basic catchment properties. This has no bearing on the main results of our fitting analysis, but is deemed important if the main interest in application of these models is to estimate the FDCs of ungaged watersheds. To analyze the regionalization potential of each FDC model we relate the optimized coefficients to basic catchment properties of the MOPEX data set. The list of basin descriptions is available on the internet from the ftp site of the MOPEX data set. We restrict attention to catchment properties that are relatively easy to derive, including watershed area, the ratios of annual precipitation and annual potential evaporation, annual runoff and annual precipitation, and annual runoff and annual potential evaporation, NDVI value, porosity, the upper limit of the unsaturated soil moisture content, the wilting point, the saturated hydraulic conductivity, the annual potential evapotranspiration, the annual precipitation, the fractions of sand, loamy sand, sandy loam, and silt loam in the upper 10 cm of the soil, the fraction of mixed forest, the coverage of closed shrublands, and the fraction of woodland and wooded grassland. Most of these descriptors are unitless.

We select those five basin descriptors that exhibit the highest linear correlation with each parameter of each model. Multivariate linear regression (MLR) is then used to combine those five catchment properties into a single equation. In so doing, we divide the pool of 438 MOPEX watersheds into a calibration and evaluation data set. We remove watersheds with a significant number of zero flow days. This leaves us with 177 watersheds for calibration and 181 watersheds for evaluation. The MLR function is derived for the 177 calibration watersheds, and subsequently evaluated for the 181 evaluation watersheds.

Table 5 summarizes the results of our regionalization analysis. The second and third column list the performance of each model for the calibration and evaluation data set. The last column summarizes for each parameter of each FDC model the index of the basin descriptor. This should help readers implement the regionalization functions in their own work. The listed RMSE values measure the distance between the empirical FDC and simulated FDC derived using values of the model parameters predicted by the MLR equation using values of the basin descriptors. Values listed in parenthesis display the performance when evaluated in the exceedance probability space.

The results of this Table demonstrate that the 2-parameter LN model achieves the best regionalization results. The average RMSE amounts to about 0.69 (mm/day) and 0.10 (–) when evaluated in the streamflow and exceedance probability space, respectively. The GEV model exhibits very similar RMSE values in the streamflow space (0.69 mm/day) but somewhat larger values of 0.17 (–) when the model misfit is measured in the exceedance probability space. The GP model also shows a relatively high regionalization potential. The proposed VG model exhibits rather poor regionalization relationships with RMSE value that is 3–5 times larger than that of the 2-parameter LN model when evaluated in the streamflow space. The result of the K model is somewhat better but still much inferior to that of the LN model. These findings are rather disappointing and highlight a trade-off between quality of fit and regionalization potential.

Note that the results of the K-2 model do not match those of the 2-parameter LN distribution, even though their functions are mathematically equivalent after some simple transformation of their parameters. This finding highlights one of the limitations of MLR and that is that it can capture only linear relationships between the model parameters and catchment properties. Parameter transformations that enhance linearity between their optimized values and catchment properties will improve regionalization relationships.

One of the reasons to use the WRF of K is that its parameters can be directly related to the pore size distribution, and thus have a physical interpretation. We verify whether this also holds for the formulations used herein to fit the empirical FDCs of the MOPEX watersheds. The optimized values of a_K and b_K of the K-2 model indeed show a strong correlation with the physical and climatologic characteristics of the watershed. Linear correlation coefficients of about 0.8 are found with the mean annual precipitation and potential evapotranspiration. This opens up new possibilities for regionalization and prediction in ungaged basins using for instance, precipitation data products from remote sensing. Note that the coefficient a_K of the 2-parameter K model exhibits an almost perfect linear correlation with the median streamflow value (see Fig. 12). This result is not surprising as the parameter a_K is defined as the median streamflow value.

Now we have established an almost perfectly linear correlation between the median streamflow level and the value of parameter a_K of the 2-parameter K model, we can readily fit this model to empirical FDCs. Note, the correlation between a_K and the median streamflow level is not perfectly linear (r = 0.997). We can therefore get a somewhat improved fit to the empirical FDC if we fine tune a_K and b_K jointly.

Table 5
Performance statistics of each model in our regionalization analysis. The RMSE values are derived by comparing for each model separately the empirical FDC with the simulated FDC derived using model parameter values derived from the regionalization equations of MLR with the five most informative basin descriptors. Listed values in column 2 and 3 correspond to the average error in the streamflow (Table 1) and (between brackets) exceedance probability (Table 2) space. The five catchment properties that exhibit the highest correlation with each model parameter (optimized in the streamflow space) are listed in the last column.

Model name	Calibration set	Evaluation set	Basin descriptors (Y-space)
Lognormal-2	0.7031 (0.1060)	0.6929 (0.0989)	a_{LN} : 19 18 51 52 17[a] b_{LN} : 51 23 19 26 18
Gumbel	1.1200 (0.1401)	1.1205 (0.1253)	a_G : 81 26 23 22 21 b_G : 26 81 82 23 169
Logistic	1.3451 (0.1448)	1.3439 (0.1323)	a_{LG} : 52 17 18 19 51 b_{LG} : 52 17 18 19 51
Logarithmic	0.9792 (0.1201)	1.0078 (0.1220)	a_{LOG} : 52 17 18 19 51 b_{LOG} : 21 22 81 23 26
Power	1.0178 (3.2974)	1.0432 (3.2072)	a_P : 51 23 19 26 81 b_P : 52 17 18 19 51
Quimpo	1.7517 (0.4208)	1.5779 (0.4704)	a_Q : 52 17 4 23 26 b_Q : 51 189 19 18 20
Viola	0.8748 (0.5618)	0.8884 (0.6232)	a_V : 52 17 18 19 51 b_V : 51 23 26 19 81
VG-2	2.9013 (0.2161)	3.1861 (0.2043)	a_{VG} : 20 19 18 52 189 b_{VG} : 170 23 22 21 52
Kosugi-2	0.8057 (0.1284)	0.8669 (0.1156)	a_K : 52 17 18 19 51 b_K : 51 23 19 26 18
Lognormal-3	0.7405 (0.1119)	0.7463 (0.1083)	a_{LN} : 19 18 51 17 52 b_{LN} : 51 19 23 26 18 c_{LN} : 170 21 17 22 23
Generalized Pareto	0.7202 (0.1496)	0.7668 (0.1327)	a_{GP} : 170 21 22 23 26 b_{GP} : 52 17 18 19 51 c_{GP} : 51 26 81 23 19
GEV	0.6938 (0.2057)	0.7649 (0.1651)	a_{GEV} : 52 17 18 19 51 b_{GEV} : 52 17 18 19 51 c_{GEV} : 51 26 23 19 81
Franchini and Suppo	1.3560 (0.1602)	1.3626 (0.1535)	a_{FS} : 52 17 4 18 26 b_{FS} : 52 18 17 19 51 c_{FS} : 51 189 19 18 20
VG-3	1.9910 (0.2696)	1.9842 (0.2979)	a_{VG} : 20 19 18 189 52 b_{VG} : 20 19 189 18 52 c_{VG} : 52 17 18 170 19
Kosugi-3	0.9623 (0.1429)	0.9637 (0.8980)	a_K : 52 17 18 19 51 b_K : 51 19 23 26 18 c_K : 170 21 17 22 23

[a] 4: area, 17: rainfall/PET ratio, 18: runoff/rainfall ratio, 19: ET/PET ratio, 20: NDVI derivative value, 21: porosity, 22: upper limit of unsaturated soil water content, 23: wilting point, 26: saturated hydraulic conductivity, 51: annual PET, 52: annual rainfall, 81: fraction of sand (0–10 cm layer), 82: loamy sand fraction upper 10 cm of soil, 83: sandy loam fraction (0–10 cm), 169: fraction of mixed forest coverage, 170: fraction of closed shrublands coverage, 189: fraction of wooded grassland coverage.

5. Conclusions

The FDC has been used to characterize information regarding catchment streamflow variability and flow regime in various hydrologic design and management studies. While several physically-based and probabilistic/mathematical functions have been used to model the empirical FDCs, they fail to characterize adequately the low tail of the FDC at high exceedance probabilities, and the large differences between the FDCs of watersheds with contrasting hydrologic behaviors. This paper extends the work of Vrugt and Sadegh (2013) and introduces a new class of closed-form parametric expressions to closely characterize the FDCs of arid, semi-arid, and wet catchments. These continuous functions, equivalent to the WRFs of VG and K, are derived from the field of vadose zone hydrology and have been used widely to describe the water characteristic of variably saturated soils. Two different formulations of the VG and K models have been introduced to mimic empirical FDCs. These functions differ in their structural complexity and include between two to three coefficients whose values need to be derived by fitting against the observed FDCs.

Application of the WRFs to 430 watersheds of the MOPEX data set demonstrates that the VG and K models closely match the empirical FDCs of arid, semi-arid, and wet catchments. The proposed parametric expressions exhibit a superior performance over other commonly used FDC models in the hydrologic literature. If quality of fit is of paramount importance then the 3-parameter VG model is preferred as it provides the closest fit to the empirical FDCs. If the fitting coefficients of the FDC model are to be used for regionalization or as summary statistics in diagnostic analysis then the 2-parameter LN function (K) is preferred.

It is further demonstrated that the proposed parametric expressions exhibit a rather poor regionalization potential. The 2-parameter LN model achieves the best regionalization performance from all FDC models considered in our analysis. The parameters a_K and b_K of the K-2 model exhibit a strong correlation however with physical and climatological characteristics of the catchment. What is more, the parameter a_K is nearly equivalent to the median value of the streamflow observations, reducing the K-2 calibration problem to just a single parameter.

Acknowledgments

The first and second author appreciate the support and funding from the UC-Lab Fees Research Program Award 237825. The MATLAB code of FDCFIT can be obtained from the second author upon request, (jasper@uci.edu). The MOPEX data set is freely available and can be downloaded from the following website: http://ftp://hydrology.nws.noaa.gov/pub/gcip/mopex/US_Data/.

References

Blazkova, S., Beven, K., 2009. A limits of acceptability approach to model evaluation and uncertainty estimation in flood frequency estimation by continuous simulation: Skalka catchment, Czech Republic. Water Resour. Res. 45, W00B16. http://dx.doi.org/10.1029/2007WR006726.

Booker, D.J., Snelder, T.H., 2012. Comparing methods for estimating flow duration curves at ungauged sites. J. Hydrol. 434–435, 78–94.
Botter, G., Zanardo, S., Porporato, A., Rodriguez-Iturbe, I., Rinaldo, A., 2008. Ecohydrological model of flow duration curves and annual minima. Water Resour. Res. 44, W08418. http://dx.doi.org/10.1029/2008WR006814.
Brown, A.E., Western, A.W., McMahon, T.A., Zhang, L., 2013. Impact of forest cover changes on annual streamflow and flow duration curves. J. Hydrol. 483, 39–50.
Castellarin, A., Galeati, G., Brandimarte, L., Montanari, A., Brath, A., 2004a. Regional flow-duration curves: reliability for ungauged basins. Adv. Water Resour. 27, 953–965.
Castellarin, A., Vogel, R.M., Brath, A., 2004b. A stochastic index flow model of flow duration curves. Water Resour. Res. 40, W03104. http://dx.doi.org/10.1029/2003WR002524.
Castellarin, A., Camorani, G., Brath, A., 2007. Predicting annual and long-term flow-duration curves in ungauged basins. Adv. Water Resour. 30, 937–953. http://dx.doi.org/10.1016/j.advwatres.2006.08.006.
Cheng, L., Yaeger, M., Viglione, A., Coopersmith, E., Ye, S., Sivapalan, M., 2012. Exploring the physical controls of regional patterns of flow duration curves part 1: insights from statistical analyses. Hydrol. Earth Syst. Sci. 16, 4435–4446. http://dx.doi.org/10.5194/hess-16-4435-2012.
Chow, V.T., 1964. Handbook of Applied Hydrology. Mc-Graw Hill BookCo., New York, NY.
Cigizoglu, H.K., Bayazit, M., 2000. A generalized seasonal model for flow duration curve. Hydrol. Process. 14, 1053–1067.
Cole, R.A.J., Johnston, H.T., Robinson, D.J., 2003. The use of flow duration curves as a data quality tool. Hydrol. Sci. J. 48 (6), 939–951.
Coopersmith, E., Yaeger, M.A., Ye, S., Cheng, L., Sivapalan, M., 2012. Exploring the physical controls of regional patterns of flow duration curves part 3: a catchment classification system based on regime curve indicators. Hydrol. Earth Syst. Sci. 16, 4467–4482. http://dx.doi.org/10.5194/hess-16-4467-2012.
Croker, K.M., Young, A.R., Zaidman, M.D., Rees, H.G., 2003. Flow duration curve estimation in ephemeral catchments in Portugal. Hydrol. Sci. J. 48 (3), 427–439. http://dx.doi.org/10.1623/hysj.48.3.427.45287.
Dingman, S.L., 1978. Sythesis of flow-duration curves for unregulated streams in new hampshire. Water Resour. Bull. 14 (6), 1481–1502.
Duan, Q. et al., 2006. Model Parameter Estimation Experiment (MOPEX): an overview of science strategy and major results from the second and third workshops. J. Hydrol. 320 (12), 3–17, <http://dx.doi.org/10.1016/j.jhydrol.2005.07.031>.
Durner, W., 1994. Hydraulic conductivity estimation for soils with heterogeneous pore structure. Water Resour. Res. 30 (2), 211–223.
Euser, T., Winsemius, H.C., Hrachowitz, M., Fenicia, F., Uhlenbrook, S., Savenije, H.H.G., 2013. A framework to assess the realism of model structures using hydrological signatures. Hydrol. Earth Syst. Sci. 17, 1893–1912. http://dx.doi.org/10.5194/hess-17-1893-2013.
Fennessey, N., Vogel, R.M., 1990. Regional flow-duration curves for ungauged sites in Massachusetts. J. Water Resour. Plann. Manage. 116, 530–549.
Foster, H.A., 1934. Duration curves. ASCE Trans. 99, 1213–1267.
Franchini, M., Suppo, M., 1996. Regional analysis of flow duration curves for a limestone region. Water Resour. Manage. 10, 199–218.
Ganora, D., Claps, P., Laio, F., Viglione, A., 2009. An approach to estimate nonparametric flow duration curves in ungauged basins. Water Resour. Res. 45, W10418. http://dx.doi.org/10.1029/2008WR007472.
Gupta, H.V., Wagener, T., Liu, Y., 2008. Reconciling theory with observations: elements of a diagnostic approach to model evaluation. Hydrol. Process. 22 (18), 3802–3813.
Gupta, H.V., Clark, M.P., Vrugt, J.A., Abramowitz, G., Ye, M., 2012. Towards a comprehensive assessment of model structural adequacy. Water Resour. Res. 48, W08301. http://dx.doi.org/10.1029/2011WR011044.
Hashmi, M.Z., Shamseldin, A.Y., 2014. Use of gene expression programming in regionalization of flow duration curve. Adv. Water Resour. 68, 1–12.
Holmes, M.G.R., Young, A.R., Gustard, A., Grew, R., 2002. A region of influence approach to predicting flow duration curves within ungauged catchments. Hydrol. Earth Syst. Sci. 6, 721–731. http://dx.doi.org/10.5194/hess-6-721-2002.
Hughes, D.A., Smakhtin, V., 1996. Daily flow time series patching or extension: a spatial interpolation approach based on flow duration curves. Hydrol. Sci. J. 41 (6), 851–871. http://dx.doi.org/10.1080/02626669609491555.
Iacobellis, V., 2008. Probabilistic model for the estimation of T year flow duration curves. Water Resour. Res. 44, W02413. http://dx.doi.org/10.1029/2006WR005400.
Jehng-Jung, K., Bau, S.F., 1996. Risk analysis for flow duration curve based seasonal discharge management programs. Water Res. 30 (6), 1369–1376.
Katz, R.W., Parlange, M.B., Naveau, P., 2002. Statistics of extremes in hydrology. Adv. Water Resour. 25 (812), 1287–1304.
Kavetski, D., Fenicia, F., Clark, M.P., 2011. Impact of temporal data resolution on parameter inference and model identification in conceptual hydrological modeling: insights from an experimental catchment. Water Resour. Res. 47, W05501. http://dx.doi.org/10.1029/2010WR009525.
Kosugi, K., 1994. Three-parameter lognormal distribution model for soil water retention. Water Resour. Res. 30 (4), 891–901.
Kosugi, K., 1996. Lognormal distribution model for unsaturated soil hydraulic properties. Water Resour. Res. 32 (9), 2697–2703.
Kunkle, G.R., 1962. The baseflow-duration curve, a technique for the study of groundwater discharge from a drainage basin. J. Geophys. Res. 67 (4), 1543–1554.
Lane, P.N.J., Best, A.E., Hickel, K., Zhang, L., 2005. The response of flow duration curves to afforestation. J. Hydrol. 310, 253–265.
Leboutillier, D.W., Waylen, P.R., 1993. A stochastic model of flow duration curves. Water Resour. Res. 29 (10), 3535–3541.
Li, M., Shao, Q., Zhang, L., Chiew, F.H.S., 2010. A new regionalization approach and its application to predict flow duration curve in ungauged basins. J. Hydrol. 389 (12), 137–145.
Longobardi, A., Villani, P., 2013. A statistical, parsimonious, empirical framework for regional flow duration curve shape prediction in high permeability Mediterranean region. J. Hydrol. 507, 174–185.
Male, J.W., Ogawa, H., 1984. Tradeoffs in water quality management. Water Resour. Plan. Manage. 110 (4), 434–444.
Mallory, S.J.L., McKenzie, R.S., 1993, Water resources modeling of flow diversions. In: Proceedings of the Sixth South African National Hydrology Symposium, Pietermarietzburg, South Africa, vol. 1, pp. 429–436.
Marquardt, D., 1963. An algorithm for least-squares estimation of nonlinear parameters. J. Soc. Ind. Appl. Math. 11 (2), 431–441.
Masih, I., Uhlenbrook, S., Maskey, S., Ahmad, M.D., 2010. Regionalization of a conceptual rainfallrunoff model based on similarity of the flow duration curve: a case study from the semi-arid Karkheh basin, Iran. J. Hydrol. 391, 188–201.
McKay, M.D., Beckman, R.J., Conover, W.J., 1979. A comparison of three methods for selecting values of input variables in the analysis of output from a computer code. Technometrics 21 (2), 239–245. http://dx.doi.org/10.2307/1268522.
Mendicino, G., Senatore, A., 2013. Evaluation of parametric and statistical approaches for the regionalization of flow duration curves in intermittent regimes. J. Hydrol. 480, 19–32.
Mimikou, M., Kaemaki, S., 1985. Regionalization of flow duration characteristics. J. Hydrol. 82, 77–91.
Mitchell, W.D., 1957, Flow Duration Curves of Illinois Streams. Illinois Department of Public Works and Buildings, Division of Waterways.
Moftakhari, H.R., Jay, D.A., Talke, S.A., Kukulka, T., Bromirski, P.D., 2013. A novel approach to flow estimation in tidal rivers. Water Resour. Res. 49, 4817–4832. http://dx.doi.org/10.1002/wrcr.20363.
Moftakhari, H.R., Jay, D.A., Talke, S.A., Schoellhamer, D.H., 2015. Estimation of historic flows and sediment loads to San Francisco Bay, 18492011. J. Hydrol. 529, 1247–1261.
Moftakhari, H.R., 2015, A Novel Approach to Flow and Sediment Transport Estimation in Estuaries and Bays, PhD Thesis. Portland State University.
Mohamoud, Y.M., 2008. Prediction of daily flow duration curve and streamflow for ungauged catchments using regional flow duration curves. Hydrolog. Sci. J. 53, 706–724. http://dx.doi.org/10.1623/hysj.53.4.706.
Nelder, J.A., Mead, R., 1965. A simplex method for function minimization. Comput. J. 7, 308–313.
Niadas, I.A., 2005. Regional flow duration curve estimation in small ungauged catchments using instantaneous flow measurements and a censored data approach. J. Hydrol. 314, 48–66.
Niadas, I.A., Mentzelopoulos, P.G., 2008. Probabilistic flow duration curves for small hydro plant design and performance evaluation. Water Resour. Manage. 22, 509–523.
Pfannerstill, M., Guse, B., Fohrer, N., 2014. Smart low flow signature metrics for an improved overall performance evaluation of hydrological models. J. Hydrol. 510, 447–458.
Pitman, W.V., 1993, Simulation of run-of-river schemes using monthly data. In: Proceedings of the Sixth South African Hydrology Symposium, Pietermarietzburg, South Africa, vol. 1, pp. 445–452.
Pugliese, A., Castellarin, A., Brath, A., 2014. Geostatistical prediction of flowduration curves in an index-flow framework. Hydrol. Earth Syst. Sci. 18, 3801–3816.
Pumo, D., Noto, L.V., Viola, F., 2013. Ecohydrological modelling of flow duration curve in Mediterranean river basins. Adv. Water Resour. 52, 314–327.
Quimpo, R.G., Alejandrino, A.A., McNally, T.A., 1983. Regionalised flow duration curves for Philippines. J. Water Resour. Plan. Manage. 109 (4), 320–330.
Refsgaard, J.C., Knudsen, J., 1996. Operational validation and intercomparison of different types of hydrological models. Water Resour. Res. 32, 2189–2202.
Sadegh, M., Vrugt, J.A., 2014. Approximate Bayesian computation using Markov chain Monte Carlo simulation: DREAM$_{(ABC)}$. Water Resour. Res. 50, 6767–6787. http://dx.doi.org/10.1002/2014WR015386, 2014a.
Sadegh, M., Vrugt, J.A., Xu, C., Volpi, E., 2015. The stationarityparadigm revisited: Hypothesis testingusing diagnostics, summary metrics, and DREAM$_{(ABC)}$. Water Resour. Res. 51. http://dx.doi.org/10.1002/2014WR016805.
Sauquet, E., Catalogne, C., 2011. Comparison of catchment grouping methods for flow duration curve estimation at ungauged sites in France. Hydrol. Earth Syst. Sci. 15, 2421–2435.
Sawicz, K., Wagener, T., Sivapalan, M., Troch, P.A., Carrillo, G., 2011. Catchment classification: empirical analysis of hydrologic similarity based on catchment function in the eastern USA. Hydrol. Earth Syst. Sci. 15, 2895–2911.
Schaefli, B., Gupta, H.V., 2007. Do Nash values have value? Hydrol. Processes 21, 2075–2080.
Searcy, J.K., 1959, Flow-duration curves, Water Supply Paper 1542-A, U.S. Geological Survey, Reston, Virginia.
Singh, K.P., 1971. Model flow duration and streamflow variability. Water Resour. Res. 7 (4), 1031–1036.
Singh, R.D., Mishra, S.K., Chowdhary, H., 2001. Regional flow-duration models for large number of ungauged Himalayan catchments for planning microhydro projects. J. Hydrol. Eng. 6 (4), 310–316.
Sivapalan, M., Takeuchi, K., Franks, S.W., Gupta, V.K., Karambiri, H., Lakshmi, V., Liang, X., McDonnell, J.J., Mendiondo, E.M., O'Connell, P.E., Oki, T., Pomeroy, J.W., Schertzer, D., Uhlenbrook, S., Zehe, E., 2003. IAHS decade on predictions in ungauged basins (PUB), 20032 012: Shaping an exciting future for the

hydrological sciences. Hydrolog. Sci. J. 48, 857–880. http://dx.doi.org/10.1623/hysj.48.6.857.51421.
Smakhtin, V.U., 2001. Low flow hydrology: a review. J. Hydrol. 240, 147–186.
Son, K., Sivapalan, M., 2007. Improving model structure and reducing parameter uncertainty in conceptual water balance models through the use of auxiliary data. Water Resour. Res. 43, W01415. http://dx.doi.org/10.1029/2006WR005032.
Tharme, R.E., 2003. A global perspective on environmental flow assessment: emerging trends in the development and application of environmental flow methodologies for rivers. River Res. Appl. 19, 397–441. http://dx.doi.org/10.1002/rra.736.
van Genuchten, M.T., 1980. A closed-form equation for predicting the hydraulic conductivity of unsaturated soils. Soil Sci. Soc. Am. J. 44 (5), 892–898.
Viola, F., Noto, L.V., Cannarozzo, M., La Loggia, G., 2011. Regional flow duration curves for ungauged sites in Sicily. Hydrol. Earth Syst. Sci. 15, 323–331.
Vogel, R.M., Fennessey, N.M., 1994. Flow-duration curves I: new interpretation and confidence intervals. J. Water Resour. Plan. Manage. 120 (4), 485–504.
Vogel, R.M., Fennessey, N.M., 1995. Flow-duration curves II: a review of applications in water resources planning. Water Resour. Bull. 31 (6), 1029–1039.
Vrugt, J.A., Bouten, W., Gupta, H.V., Sorooshian, S., 2002. Toward improved identifiability of hydrologic model parameters: the information content of experimental data. Water Resour. Res. 38 (12), 1312. http://dx.doi.org/10.1029/2001WR001118.
Vrugt, J.A., Robinson, B.A., Vesselinov, V.V., 2005. Improved inverse modeling of ow and transport in subsurface media: Combined parameter and state estimation. Geophys. Res. Lett. 32, L18408. http://dx.doi.org/10.1029/2005GL023940.
Vrugt, J.A., ter Braak, C.J.F., Gupta, H.V., Robinson, B.A., 2008. Equifinality of formal (DREAM) and informal (GLUE) Bayesian approaches in hydrologic modeling? Stoch. Env. Res. Risk Assess. 23 (7), 1011–1026. http://dx.doi.org/10.1007/s00477-008-0274-y.
Vrugt, J.A., ter Braak, C.J.F., Diks, C.G.H., Higdon, D., Robinson, B.A., Hyman, J.M., 2009. Accelerating Markov chain Monte Carlo simulation by differential evolution with self-adaptive randomized subspace sampling. Int. J. Nonlinear Sci. Numer. Simul. 10 (3), 273–290.
Vrugt, J.A., Sadegh, M., 2013. Toward diagnostic model calibration and evaluation: approximate Bayesian computation. Water Resour. Res. 49, 1–11. http://dx.doi.org/10.1002/wrcr.20354.
Vrugt, J.A., 2016. Markov chain Monte Carlo simulation using the DREAM software package: theory, concepts, and MATLAB Implementation. Environ. Model. Softw. 75, 273–316. http://dx.doi.org/10.1016/j.envsoft.2015.08.013.
Wagener, T., Wheater, H.S., 2006. Parameter estimation and regionalization for continuous rainfall-runoff models including uncertainty. J. Hydrol. 320, 132–154.
Warnick, C.C., 1984. Hydropower Engineering. Prentice-Hall, Inc., Englewood Cliffs, New Jersey, pp. 59–73.
Waseem, M., Shin, J., Kim, T., 2015. Comparing spatial interpolation schemes for constructing a flow duration curve in an ungauged basin. Water Resour. Manage 29, 2249–2265.
Westerberg, I.K., Guerrero, J.-L., Younger, P.M., Beven, K.J., Seibert, J., Halldin, S., Freer, J.E., Xu, C.-Y., 2011. Calibration of hydrological models using flow-duration curves. Hydrol. Earth Syst. Sci. 15, 2205–2227. http://dx.doi.org/10.5194/hess-15-2205-2011.
Westerberg, I.K., Gong, L., Beven, K.J., Seibert, J., Semedo, A., Xu, C.-Y., Halldin, S., 2014. Regional water balance modelling using flow-duration curves with observational uncertainties. Hydrol. Earth Syst. Sci. 18, 2993–3013.
Wilby, R., Greenfield, B., Glenny, C., 1994. A coupled synoptichydrological model for climate change impact assessment. J. Hydrol. 153, 265–290.
Yadav, M., Wagener, T., Gupta, H., 2007. Regionalization of constraints on expected watershed response. Adv. Water Resour. 30, 1756–1774.
Yaeger, M., Coopersmith, E., Ye, S., Cheng, L., Viglione, A., Sivapalan, M., 2012. Exploring the physical controls of regional patterns of flow duration curves part 4: a synthesis of empirical analysis, process modeling and catchment classification. Hydrol. Earth Syst. Sci. 16, 4483–4498. http://dx.doi.org/10.5194/hess-16-4483- 2012.
Ye, S., Yaeger, M., Coopersmith, E., Cheng, L., Sivapalan, M., 2012. Exploring the physical controls of regional patterns of flow duration curves part 2: role of seasonality, the regime curve, and associated process controls. Hydrol. Earth Syst. Sci. 16, 4447–4465. http://dx.doi.org/10.5194/hess-16-4447-2012.
Yilmaz, K., Gupta, H.V., Wagener, T., 2008. A process-based diagnostic approach to model evaluation: application to the NWS distributed hydrologic model. Water Resour. Res. 44, W09417. http://dx.doi.org/10.1029/2007WR006716.
Yokoo, Y., Sivapalan, M., 2011. Towards reconstruction of the flow duration curve: development of a conceptual framework with a physical basis. Hydrol. Earth Syst. Sci. 15, 2805–2819. http://dx.doi.org/10.5194/hess-15-2805-2011.
Yu, P.S., Yang, T.C., 1996. Synthetic regional flow duration curve for southern Taiwan. Hydrolog. Process. 10, 373–391.
Yu, P.S., Yang, T.C., 2000. Using synthetic flow duration curves for rainfall-runoff model calibration at ungauged sites. Hydrol. Process. 14, 117–133.
Yu, P.S., Yang, T.C., Wang, Y.C., 2002. Uncertainty analysis of regional flow duration curves. J. Water Resour. Pl. Manage. 128 (6), 424–430.
Zhang, L., Potter, N., Hickel, K., Zhang, Y., Shao, Q., 2008. Water balance modeling over variable time scales based on the Budyko framework model development and testing. J. Hydrol. 360, 117–131. http://dx.doi.org/10.1016/j.jhydrol.2008.07.021.
Zhao, F., Xu, Z., Zhang, L., 2012. Changes in streamflow regime following vegetation changes from paired catchments. Hydrol. Process. 26, 1561–1573. http://dx.doi.org/10.1002/hyp.8266.